Supporting information

Tuning the Hydrophobicity of Glycine Ester through *N*-Acylation and Introducing Quaternary Pyridinium Group Enables Selectivity against Gram-Positive Bacteria

Aleena Pious[a], Dharshini Karnan Singaravelu[a], Srimari Srikanth[a], Venkatasubramaian Ulaganathan[a], Chithra Sivanandan[b], Fadaa Alown[c], Fuad Ameen[d], Anbazhagan Veerappan[a]*

[a]School of Chemical and Biotechnology, SASTRA Deemed University, Thanjavur - 613 401, Tamil Nadu, India

[b]Department of Biotechnology of Medicines, Warsaw University of Technology, Warsaw, Poland

[c]Public Authority for Applied Education and Training (paaet), Faculty of Basic Education/Science Department. Kuwait

[d]Department of Botany and Microbiology, College of Science, King Saud University, Riyadh, 11451, Saudi Arabia

Materials and methods

2.1. Materials

Pyridine-2-carboxaldehyde, thionyl chloride was purchased from Hyma, India. Fatty acids and Glycine methyl ester were purchased from TCI, India. Triethylamine and sodium cyanoborohydride were purchased from SRL Chemicals. Methyl iodide was purchased from LOBA Chemie. Media and reagents for microbiology were obtained from Himedia India.

2.2. Synthesis of N-acyl-N-(pyridin-2-ylmethyl)glycine methyl ester (PyNAGe)

The *N*-acyl-N-(pyridin-2-ylmethyl)glycine methyl ester was synthesized from glycine. Briefly, glycine methyl ester hydrochloride (46.68 mmol), pyridine aldehyde (9.336 mmol), and sodium cyanoborohydride (23.34 mmol) were dissolved in 10 mL of methanol and allowed to react for 24 h at room temperature. The reaction progress was monitored by thin-layer chromatography. The reaction mass was extracted using ethyl acetate and a saturated solution of NH_4Cl. The crude product of methyl 2-((pyridin-2-ylmethyl)amino)acetate obtained from the organic layer was subjected to N-acylation without further purification. The acid chlorides for N-acylation were prepared freshly by reacting 1.2 equivalents of fatty acids (3.32 mmol) with 3.5 equivalents of thionyl chloride (9.709 mmol) in dichloromethane under a nitrogen atmosphere for 1 h at room temperature. The freshly prepared acid chlorides

were added dropwise to a round-bottom flask containing 1 equivalent of methyl 2-((pyridin-2-ylmethyl)amino)acetate (2.774 mmol) and 3 equivalents of triethylamine (8.322 mmol) in DCM solvent. Following the completion of the reaction, the crude mass was extracted with ethyl acetate and saturated with $NaHCO_3$. The organic layer was dried and purified by column chromatography (mesh size, 60-120). The product was eluted with ethyl acetate: hexane (30:70). The yield of the reaction is around 75%. The product was confirmed by ^{1}H and ^{13}C NMR (see supporting information).

2.3. Synthesis of 2-((N-(acylglycine ester)methyl)-1-methylpyridin-1-ium iodide (QPyNAGe)

PyNAGe was quaternized using methyl iodide. Typically, the purified PyNAGe was solubilized in 10% acetonitrile and allowed to react with two volumes of methyl iodide for 48 h at room temperature. Following the completion of the reaction, the solvent and excess methyl iodide were removed by rotary evaporator. The obtained precipitate was washed several times with acetone and hexane to obtain the pure product. The yield of the reaction is around 95%. The purity of the product was confirmed by ^{1}H NMR, ^{13}C NMR, and HRMS. (See supporting information).

2.4. Antimicrobial activity

The antimicrobial activity of the synthesized molecules was assessed by the zone of inhibition (ZOI) assay [19]. Briefly, a 0.1 OD595nm (1.0×10^8 cfu/mL, equivalent to 0.5 McFarland) bacterial culture was spread on a sterile nutrient agar plate using sterile cotton swabs. A well with a 10 mm diameter was created on the agar plate using gel puncture. About 50 µL of QPyNAGe (1 mg/mL) was loaded into the well and incubated overnight at 37 °C in a static incubator. The strains used in this study are *Staphylococcus aureus* (MTCC3160), Methicillin Susceptible *Staphylococcus aureus* (ATCC29213), Methicillin Resistant *Staphylococcus aureus* (ATCC43300), *Enterococcus feacalis* (ATCC29212), *Streptococcus iniae* (ATCC29178), *Escherichia coli* (MTCC723), Uropathogenic *Escherichia coli* (MTCC729), *Pseudomonas aeruginosa* (MTCC1688), Carbapenem Resistant *Acinetobacter baumanii* (MTCC12889), *Proteus mirabilis* (MTCC425). The formation of a zone around the well indicates antimicrobial activity.

2.5. Determination of minimum inhibitory concentration and minimum bactericidal concentration

The minimum inhibitory concentration (MIC) of all QPyNAGe was determined using turbidometry and resazurin microtiter assay (REMA) in accordance with CLSI broth

microdilution guidelines [20]. Typically, test compounds were serially diluted in LB broth in 96-well plates at concentrations ranging from 0.98 to 2000 µM. Approximately 50 µL of 1.0 × 10^8 cfu/mL (equivalent to 0.5 McFarland) bacterial cells were added to each well, and the mixture was incubated overnight at 37 °C in a shaker incubator. After overnight treatment, the turbidity in the wells was measured using an ELISA plate reader set at 595 nm. The well with the least amount of turbidity was recorded as MIC. After the turbidity was measured, the wells were treated with 50 µL of 0.01% resazurin for two hours at 37 °C. The well containing living cells appears pink, while the dead cells appear blue. The minimum bactericidal concentration (MBC) was determined by swabbing 10 µL of treated cells from the MIC plate onto an agar plate following the turbidity measurement. After overnight incubation at 37ºC, the treatment concentration with no bacterial growth was recorded as MBC. The experiments were repeated three times to test the reproducibility.

2.6. Time kill kinetics

The killing efficiency of QPyNAGe was investigated using the time kill kinetics method [21]. Briefly, 1.0×10^8 CFU/mL MRSA was treated with 7.81 µM QPyN16Ge and incubated at 37°C. Aliquots of 1.0 mL of the medium were obtained at regular intervals, and ten-fold dilutions in PBS were performed as needed. To count viable cells, 25 µL of each dilution was plated onto an LB agar plate. The bacterial colony-forming unit (CFU) was determined after 24 h incubation at 37 °C. The reference antibiotic, ciprofloxacin, was used as a positive control in the experiment, while the bacteria that were not treated with QPyN16Ge served as a negative control. Three separate experiments were conducted in triplicate, and the log CFU/mL was plotted versus time.

2.7. Hemocompatibility assay

Typically, a doctor collects 5 mL of blood from a healthy donor after obtaining informed consent. The obtained blood was immediately mixed with an equal volume of a newly prepared anticoagulant. The red blood cells (RBCs) were collected by centrifugation at 1500 rpm for five minutes. The cells were washed with PBS until the supernatant was clear. A 96-well plate containing serially diluted test compounds in PBS was mixed with 100 µL of PBS-prepared 4% RBC cells. Cells treated with 1 mM Triton X-100 and untreated cells served as positive and negative controls, respectively. The plates were incubated at 37ºC for 2 h. The hemolytic concentration (HLC) is determined by tracking cell lysis and heme release [22]. All experiments were conducted in accordance with the guidelines of the Indian Council of

Medical Research (ICMR) and were approved by the ethics committee at SASTRA University.

2.8. Membrane permeability assay

Bacterial cells grown at mid-log phase were collected by centrifugation at 3000 rpm. They were rinsed with 10 mM PBS and resuspended to prepare a bacterial suspension with an optical density (OD) at 595 nm of 0.5. The cells were treated with 1X MIC QPyNAGe for 2 h at 37 °C and then collected by centrifugation at 3000 rpm. They were washed with PBS and resuspended in PBS again. About 3 mL of treated cells were exposed to 50 µM propidium iodide (PI), and the fluorescence was measured at an emission wavelength of 617 nm, with excitation at 535 nm. Untreated cells and cells treated with 1 mM Triton X-100 were used as the negative control and positive control, respectively. The percent membrane permeability was calculated using equation 1 [23].

$$\% \text{ membrane permeability} = [(F_s - F_n)/(F_p - F_n)] \times 100 \quad (1)$$

Where, F_n is the initial PI fluorescence from the untreated cells, F_s and F_p are the PI fluorescence from the cells treated with QPyNAGe and Triton X-100, respectively.

2.9. Cytoplasmic membrane depolarization assay

Bacterial cells grown at mid-log phase were collected by centrifugation at 3000 rpm and washed with a 1:1 ratio of HEPES (5 mM) and sucrose (250 mM). Finally, the pellets were resuspended in 5 mM HEPES buffer containing 250 mM sucrose and 5 mM $MgSO_4$, pH 7.2. Then, the cells were treated with 3 µM of the membrane potential-sensitive fluorescent dye 3,3'-dipropylthiacarbocyanine iodide (DiSC3(5)) and incubated in the dark at 37 °C for 1 h. After incubation, the unbound dyes were removed by washing with HEPES buffer. About 500 µL of dye-loaded cells were treated with 1X MIC QPyNAGe for 10 min. After treatment, the fluorescent emission was recorded at 670 nm by exciting at 622 nm. Untreated cells and cells treated with 2 mM Triton X-100 were used as negative and positive controls, respectively. The percentage membrane depolarization was calculated using equation 1.

2.10. Reactive oxygen species assay

About 0.5 OD_{595nm} mid-log phase grown bacterial cells, suspended in PBS, were treated with 1X MIC QPyNAGe and incubated at 37 °C for 2 h. After treatment, the cells were centrifuged at 3000 rpm and washed three times with PBS. The pellet was suspended in 1 mL of PBS buffer containing 10 µM 2'-7'-dichlorodihydrofluorescein diacetate (DCFH-DA) and incubated at 37 °C for 30 min. After incubation, fluorescence emission was observed at 525

nm (excitation wavelength: 485 nm). The negative and positive controls were untreated cells and cells treated with 10 µL of 30% hydrogen peroxide [24].

2.11. Molecular docking and Molecular dynamics simulation

The three-dimensional crystal structures of *S. aureus* enzymes were retrieved from the Protein Data Bank (https://www.rcsb.org) using their respective PDB IDs: Aminoacyltransferase FemA (1LRZ) [25], Penicillin-binding protein 2 (1MWT) [26], Monofunctional glycosyltransferase (3VMT, 6FTB) [27, 28]. The proteins were prepared for molecular docking using the 'Protein Preparation Wizard' in Maestro. The preparation steps include adding missing hydrogen atoms and assigning bond orders. Then, the missing residues were built using Prime. The protonation states of ionizable residues were set to pH 7.0 ± 2.0 using the Epik program. Energy minimization was carried out using the OPLS4 force field [40].

The chemical structures of the ligands, QPyN18Me, QPyN16Me, QPyN12Me, QPyN10Me, and QPyN14Me were drawn using Maestro 2D sketcher. The generated 2D structures were converted into 3D conformations using the 'LigPrep' module. Ligands were energy-minimized with the OPLS4 force field.

The binding site of the prepared proteins was identified using the SiteMap module in Maestro. A receptor grid was generated using 'Receptor Grid Generation' around the predicted binding sites, and the prepared ligands were docked using the Glide extra precision (XP) docking protocol with default parameters. Among the docked complexes, top top-scoring protein–ligand complex was selected for further analysis based on the docking score.

Molecular dynamics (MD) simulations were carried out for both the apo form and the ligand-bound complex using the 'Desmond' module. The system was solvated in a cubic box using the SPC water model, neutralized with counterions to mimic physiological conditions. The systems were minimized and equilibrated using the default relaxation protocol. Production MD simulations were performed for 200 ns for each system using the OPLS4 force field. Trajectories were recorded for post-simulation analysis of structural stability and protein–ligand interactions.

2.12. Resistant testing

The ability of bacteria to develop resistance to QPyNAGe was assessed by determining MIC after repeated exposure to the drug [29]. Ciprofloxacin (Cip) was used as the standard antibiotic control. Typically, 1.0×10^8 cfu/mL S. aureus was treated with QPyN16Ge and

Cip, and their MICs were calculated as described above. After noting the MIC, *S. aureus* was exposed to 0.5X MIC for 8 h at 37°C. This process induces selective pressure, causing bacteria to acquire resistance. Following treatment, the cells were centrifuged, and their MIC was determined as previously described. The MIC established in the prior phase was utilized to set the next passage at 0.5X MIC. The experiment was repeated 29 times with repeated exposure at 0.5X MIC. The increase in the MIC indicates the development of resistance.

2.13. Animal testing

The therapeutic efficacy of QPyNAGe was evaluated using a zebrafish animal model, following the procedure described in ref. [30]. The experiments were approved by the Institutional Ethics Committee (CPCSEA-493/SASTRA/IAEC/RPP) of SASTRA University, India, conducted in accordance with the guidelines for laboratory animal facilities set by CPCSEA (Central Act 26 of 1982). Healthy adult zebrafish were obtained from the local aquarium in Thanjavur, allowed to acclimate to the lab environment, and found to be healthy after a week in the lab. For experiments, twenty healthy fish were infected intramuscularly with 10 µL of 1.0×10^8 cfu/mL MRSA and allowed 3 h to spread the infection. Following 3 h of infection, the fish were divided into the two groups. Group A serves as a control, receives a 10 µL PBS injection intramuscularly. Group B was treated with 10 µL of 7.8 µM QPyN16Ge. After treatment, the fish were collected at defined time intervals from both groups, scarified, and their muscle tissue was dissected from the opposite side of the bacterial injection. About 30 mg of the muscle tissue was homogenized, diluted appropriately, and plated on a nutrient agar plate. The plates were incubated at 37 ˚C for 12 h, and the colonies formed on the plate were counted and reported as CFU/mL.

Characterization of QPyNAGe:

N-decanoyl-N-(pyridin-2-ylmethyl)glycine methyl ester (PyN10Ge). ^{1}H NMR (600 MHz, $CDCl_3$) δ 8.58 (1H, ddd, *J* = 4.8, 1.8, 1 Hz), 7.71 (1H, td, *J* = 7.6, 1.8 Hz), 7.26 (1H, dt, *J* = 7.8, 1 Hz), 7.23 (1H, ddd, *J* = 7.6, 4.8, 1.2 Hz), 4.72 (2H, s), 4.16 (2H, s), 3.72 (3H, s), 2.45-2.39 (2H, m), 1.68 – 1.63 (2H, m), 1.34-1.20 (18H, m), 0.87 (3H, td, *J* = 7, 3.4 Hz). ^{13}C NMR (125 MHz, $CDCl_3$) δ 174.30, 169.87, 156.55, 149.85, 137.03, 122.66, 120.84, 54.14, 52.05, 47.85, 32.94, 31.82, 29.39, 29.36, 29.28, 29.26, 29.22, 25.01, 24.93, 22.61, 14.06

N-lauroyl-N-(pyridin-2-ylmethyl)glycine methyl ester (PyN12Ge). ^{1}H NMR (600 MHz, $CDCl_3$) δ 8.58 (1H, ddd, *J* = 4.8, 1.8, 1 Hz), 7.71 (1H, td, *J* = 7.8, 1.8 Hz), 7.26 (1H, d, *J* = 7.8 Hz), 7.25 – 7.22 (1H, m), 4.72 (2H, s), 4.16 (2H, s), 3.72 (3H, s), 2.45 – 2.39 (2H, m), 1.68-1.64 (2H, m), 1.34-1.20 (22H, m), 0.88 (3H, td, *J* = 7.2, 1.4 Hz). ^{13}C NMR (125 MHz,

$CDCl_3$) δ 174.31, 169.87, 156.54, 149.84, 137.04, 122.67, 120.84, 54.13, 52.05, 49.48, 47.85, 32.94, 31.85, 29.56, 29.46, 29.43, 29.36, 29.28, 29.26, 25.01, 24.93, 22.63, 14.07.

N-myristoyl-N-(pyridin-2-ylmethyl)glycine methyl ester (PyN14Ge). ^{1}H NMR (600 MHz, $CDCl_3$) δ 8.58 (1H, ddd, *J* = 4.8, 1.8, 1 Hz), 7.71 (1H, td, *J* = 7.8, 1.8 Hz), 7.25 (1H, d, *J* = 7.8 Hz), 7.23 (1H, ddd, *J* = 7.6, 4.8, 1.2 Hz), 4.72 (2H, s), 4.16 (2H, s), 3.72 (3H, s), 2.45-2.40 (2H, m), 1.69-1.63 (2H, m), 1.34-1.20 (26, m), 0.88 (3H, t, *J* = 7 Hz). ^{13}C NMR (125 MHz, $CDCl_3$) δ 174.30, 169.88, 156.58, 149.86, 137.03, 122.66, 120.85, 54.14, 52.05, 47.86, 32.95, 31.88, 29.64, 29.61, 29.58, 29.45, 29.41, 29.38, 29.31, 29.27, 25.03, 24.94, 22.65, 14.08.

N-palmitoyl-N-(pyridin-2-ylmethyl)glycine methyl ester (PyN16Ge). ^{1}H NMR (600 MHz, $CDCl_3$) δ 8.58 (1H, dt, *J* = 4.8, 1.4 Hz), 7.71 (1H, td, *J* = 7.6, 1.8 Hz), 7.26 (1H, d, *J* = 7.8 Hz), 7.23 (1H, ddd, *J* = 7.8, 4.8, 1.2 Hz), 4.72 (2H, s), 4.16 (2H,s), 3.72 (3H,s), 2.44-2.40 (2H,m), 1.69 – 1.63 (2H,m), 1.35-1.20 (30H,m), 0.88 (3H,t, *J* = 7 Hz). ^{13}C NMR (125 MHz, $CDCl_3$) δ 174.32, 169.87, 156.56, 149.84, 137.06, 122.68, 120.86, 54.13, 52.05, 47.87, 32.95, 31.88, 29.65, 29.61, 29.58, 29.45, 29.41, 29.38, 29.32, 29.27, 25.03, 22.65, 14.07.

N-stearoyl-N-(pyridin-2-ylmethyl)glycine methyl ester (PyN18Ge). ^{1}H NMR (600 MHz, $CDCl_3$) δ 8.58 (1H, dt, *J* = 4.8, 1.4 Hz), 7.71 (1H, td, *J* = 7.8, 1.8 Hz), 7.26 (1H, d, *J* = 7.8 Hz), 7.23 (1H, ddd, *J* = 7.8, 4.8, 1.2 Hz), 4.72 (2H, s), 4.16 (2H, s), 3.72 (3H, s), 2.45-2.39 (2H, m), 1.69-1.62 (2H, m)), 1.34-1.18 (34, m), 0.88 (3H, t, *J* = 3.5 Hz). ^{13}C NMR (125 MHz, $CDCl_3$) δ 174.30, 169.88, 156.59, 149.86, 137.04, 122.67, 120.85, 54.15, 52.06, 47.86, 32.96, 31.90, 29.67, 29.63, 29.60, 29.47, 29.43, 29.38, 29.33, 29.28, 25.04, 22.66, 14.09.

2-((N-(2-methoxy-2-oxoethyl)decanamido)methyl)-1-methylpyridin-1-ium (QPyN10Ge). ^{1}H NMR (600 MHz, $CDCl_3$) δ 8.95 (1H, dd, *J* = 6.2, 1.6 Hz), 8.34 (1H, td, *J* = 7.8, 1.6 Hz), 8.12 (1H, dd, *J* = 8.2, 1.6 Hz), 7.86 (1H, ddd, *J* = 7.8, 6.0, 1.6 Hz), 5.23 (2H, s), 4.67(2H, s), 4.51 (3H, s), 3.80 (3H, s), 2.33 (2H, t, *J* = 7.6 Hz), 1.62 (2H, p, *J* = 7.6 Hz), 1.34-1.21 (14H, m), 0.88 (3H, t, *J* = 7.0 Hz). ^{13}C NMR (125 MHz) δ 175.20, 169.93, 155.36, 146.29, 144.99, 127.25, 126.08, 52.88, 51.34, 49.92, 46.85, 32.78, 31.78, 29.36, 29.32, 29.19, 29.15, 24.60, 22.59, 14.04. HRMS: M.Wt calculated for $[M-I]^+$ = 349.49; Found $[M-I]^+$ = 349.2594.

2-((N-(2-methoxy-2-oxoethyl)dodecanamido)methyl)-1-methylpyridin-1-ium (QPyN12Ge). ^{1}H NMR (600 MHz, $CDCl_3$) δ 8.96 (1H, d, *J* = 6.4 Hz), 8.34 (1H, td, *J* = 8.0, 1.6 Hz), 8.12 (1H, dd, *J* = 8.2, 1.6 Hz), 7.86 (1H, ddd, *J* = 7.8, 6.0, 1.6 Hz), 5.23 (2H, s), 4.67 (2H, s), 4.51 (3H, s), 3.80 (3H,s), 2.33 (2H,t, *J* = 7.6 Hz),, 1.62 (2H, p, *J* = 7.6 Hz), 1.34-1.21 (18H, m), 0.88 (3H, t, *J* = 7.0 Hz). ^{13}C NMR (125 MHz, $CDCl_3$) δ 175.22, 169.94, 155.53, 146.18, 144.91,

127.29, 125.98, 52.87, 51.35, 50.01, 46.85, 32.78, 31.85, 29.55, 29.42, 29.34, 29.27, 29.17, 24.61, 22.63, 14.06. HRMS: M.Wt calculated for $[M-I]^+$ = 377.55; Found $[M-I]^+$ = 377.2961.

2-((N-(2-methoxy-2-oxoethyl)tetracanamido)methyl)-1-methylpyridin-1-ium (QPyN14Ge). ^{1}H NMR (600 MHz, $CDCl_3$) δ 8.98 (1H, dd, *J* = 6.2, 1.6 Hz), 8.34 (1H, td, *J* = 7.8, 1.6 Hz), 8.12 (1H, dd, *J* = 8.2, 1.6 Hz), 7.86 (1H, ddd, *J* = 7.8, 6.2, 1.6 Hz), 5.23 (2H, s), 4.67 (2H, s), 4.51 (3H,s), 3.80 (3H,s) 2.33 (2H,t, *J* = 7.6 Hz), 1.62 (2H, p, *J* =7.6 Hz), 1.34-1.21 (22H, m), 0.88 (3H, t, *J* = 7 Hz). ^{13}C NMR (125 MHz, $CDCl_3$) δ 175.21, 169.93, 155.43, 146.24, 144.94, 127.25, 126.02, 52.88, 51.34, 49.96, 46.83, 32.78, 31.85, 29.59, 29.56, 29.52, 29.42, 29.34, 29.29, 29.17, 29.09, 24.60, 22.62, 14.07. HRMS: M. Wt calculated for $[M-I]^+$ = 405.60; Found $[M-I]^+$ = 405.3160.

2-((N-(2-methoxy-2-oxoethyl)palmitamido)methyl)-1-methylpyridin-1-ium (QPyN16Ge). ^{1}H NMR (600 MHz, $CDCl_3$) δ 8.96 (1H, dd, *J* = 6.2, 1.6 Hz), 8.34 (1H, td, *J* = 8.0, 1.6 Hz), 8.12 (1H, dd, *J* = 8.2, 1.6 Hz), 7.86 (1H, ddd, *J* = 7.8, 6.0, 1.6 Hz), 5.23 (2H, s), 4.67(2H, s), 4.51 (3H, s), 3.80 (3H,s), 2.33 (2H, t, *J* = 7.6 Hz), 1.62 (2H, p, *J* = 7.6 Hz), 1.35-1.21 (26H,m), 0.88 (3H, t, *J* = 7 Hz). ^{13}C NMR (125 MHz, $CDCl_3$) δ 175.23, 169.95, 155.51, 146.17, 144.92, 127.27, 125.98, 52.89, 51.35, 50.01, 46.85, 32.79, 31.87, 29.64, 29.61, 29.58, 29.53, 29.44, 29.35, 29.31, 29.18, 24.61, 22.64, 14.08. HRMS: M. Wt calculated for $[M-I]^+$ = 433.66; Found $[M-I]^+$ = 433.3422.

2-((N-(2-methoxy-2-oxoethyl)stearamido)methyl)-1-methylpyridin-1-ium (QPyN18Ge). ^{1}H NMR (600 MHz, $CDCl_3$) δ 8.92 (1H, dd, *J* = 6.2, 1.4 Hz), 8.34 (1H, td, *J* = 8.0, 1.6 Hz), 8.15 – 8.09 (1H, m), 7.89 -7.81 (1H, m), 5.24 (2H, s), 4.68 (2H, s), 4.51 (3H, s) 3.81 (3H, s), 2.33 (2H, t, *J* = 7.6 Hz), 1.64-1.58 (2H, m), 1.33-1.21 (30H, m), 0.88 (3H, t, *J* = 7 Hz). ^{13}C NMR (125 MHz, $CDCl_3$) δ 175.21, 169.93, 155.48, 146.21, 144.93, 127.27, 126.01, 52.87, 51.35, 49.99, 46.85, 33.25, 32.79, 31.87, 29.64, 29.60, 29.58, 29.53, 29.44, 29.35, 29.30, 29.18, 29.11, 24.61, 22.63, 14.07. HRMS: M. Wt calculated for $[M-I]^+$ = 461.71; Found $[M-I]^+$ = 461.3782.

In the ^{1}H NMR analysis of QPyN18Ge, the deshielded aromatic protons were found at chemical shift values of δ8.92 (1H, dd, J = 6.2, 1.4 Hz), 8.34 (1H, td, J = 8.0, 1.6 Hz), 8.15 – 8.09 (1H, m), and 7.89 – 7.81 (1H, m). Methylene protons are present between the ester and the amide at δ4.68 (2H, s) and between the pyridine ring and the amide bond at δ5.24 (2H, s). It contains the quaternary methyl group at δ4.51 (3H, s). The methyl group of the ester functional group is observed at δ 3.81 (3H, s). The methylene group attached to the amide bond, which makes up a part of the long acyl chain length, is located at δ2.33 (3H, t, J = 7.6

Hz). The δ 1.64-1.58 (2H, m) and 1.33-1.21 (30H, m) regions include all of the additional methylene groups in the long acyl chain. The acyl chain's terminal methyl proton peaks at δ0.88 (3H, t, J = 7 Hz). In the ^{13}C NMR, the carbonyl group of the amide and the ester functional group are located at resonances of δ175.21 and δ169.93, respectively. The pyridine ring's ortho and para carbons near the nitrogen atom are less protected, and the peak was located at δ155.48, δ146.21, and δ144.93. The ring's meta carbon atoms are represented by the peaks at δ 127.27 and δ 126.01. The methylene carbon between the ester functional group and the amide group is at δ51.35, and the methylene carbon between the amide group and pyridine is at δ52.87. The carbon resulting from quaternization with methyl iodide was identified at δ49.99. The methyl carbon signal of the ester functional group is located at δ 46.85. The range of δ33 to δ22 accounts for additional methylene carbons in the long acyl chain. The shielding methyl carbon in the acyl chain is located at δ 14.07. The HRMS result of QPyN18Ge, which was calculated to be 461.3782, supports the purity of the preparation.

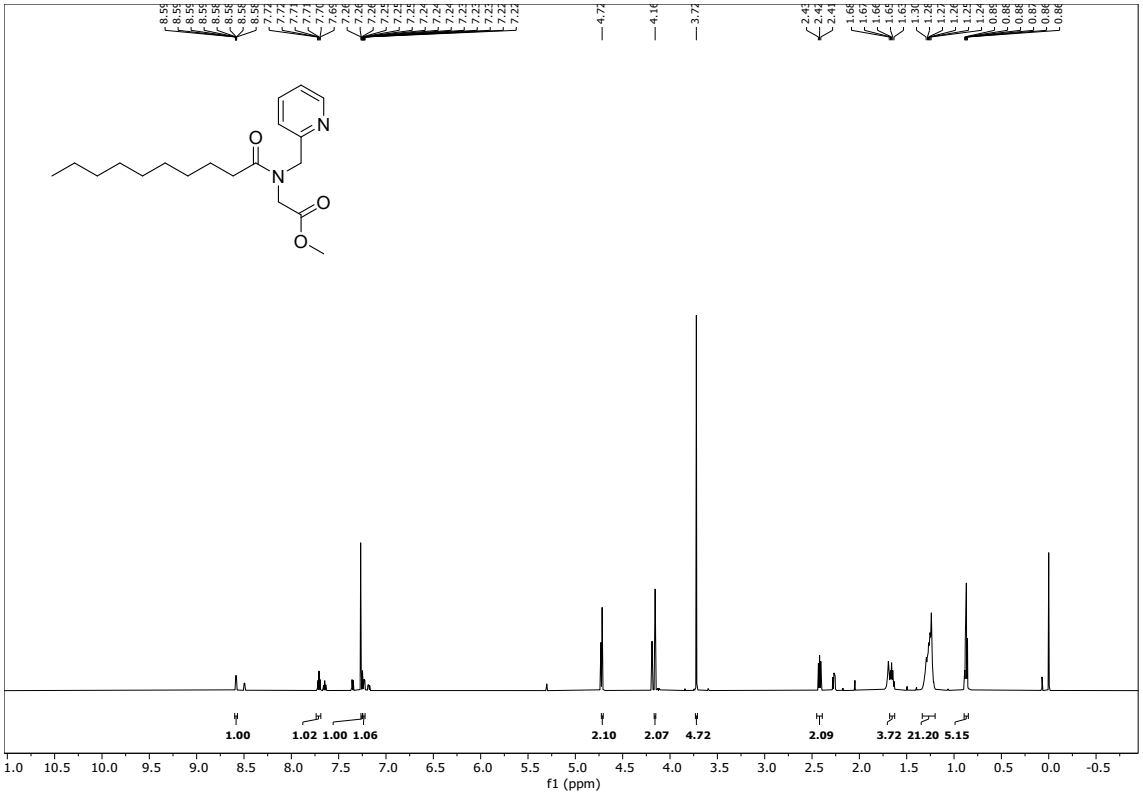

Fig. S1: *N-decanoyl-N-(pyridin-2-ylmethyl)glycine methyl ester (PyN10Ge)*. ^{1}H NMR (600 MHz, $CDCl_3$). δ 8.58 (1H, ddd, *J* = 4.8, 1.8, 1 Hz), 7.71 (1H, td, *J* = 7.6, 1.8 Hz), 7.26 (1H, dt, *J* = 7.8, 1 Hz), 7.23 (1H, ddd, *J* = 7.6, 4.8, 1.2 Hz), 4.72 (2H, s), 4.16 (2H, s), 3.72 (3H, s), 2.45-2.39 (2H, m), 1.68 – 1.63 (2H, m), 1.34-1.20 (18H, m), 0.87 (3H, td, *J* = 7, 3.4 Hz).

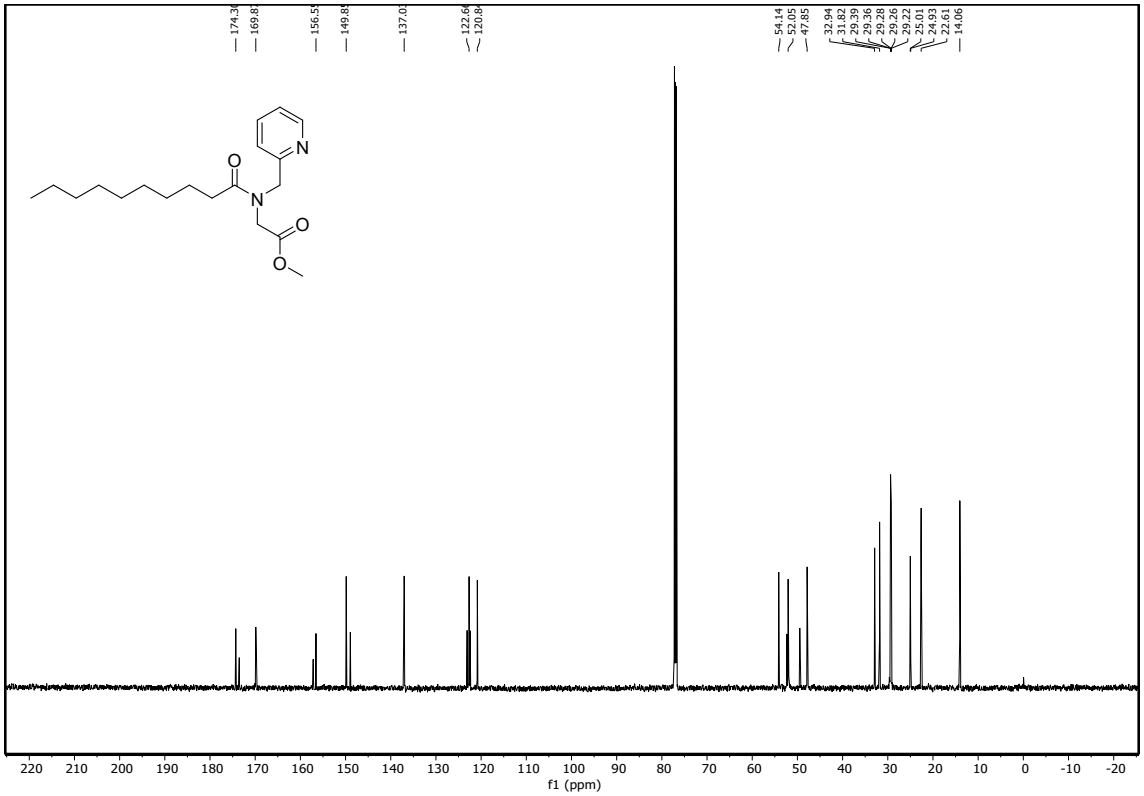

Fig. S2: PyN10Ge ^{13}C NMR (125 MHz). δ 174.30, 169.87, 156.55, 149.85, 137.03, 122.66, 120.84, 54.14, 52.05, 47.85, 32.94, 31.82, 29.39, 29.36, 29.28, 29.26, 29.22, 25.01, 24.93, 22.61, 14.06.

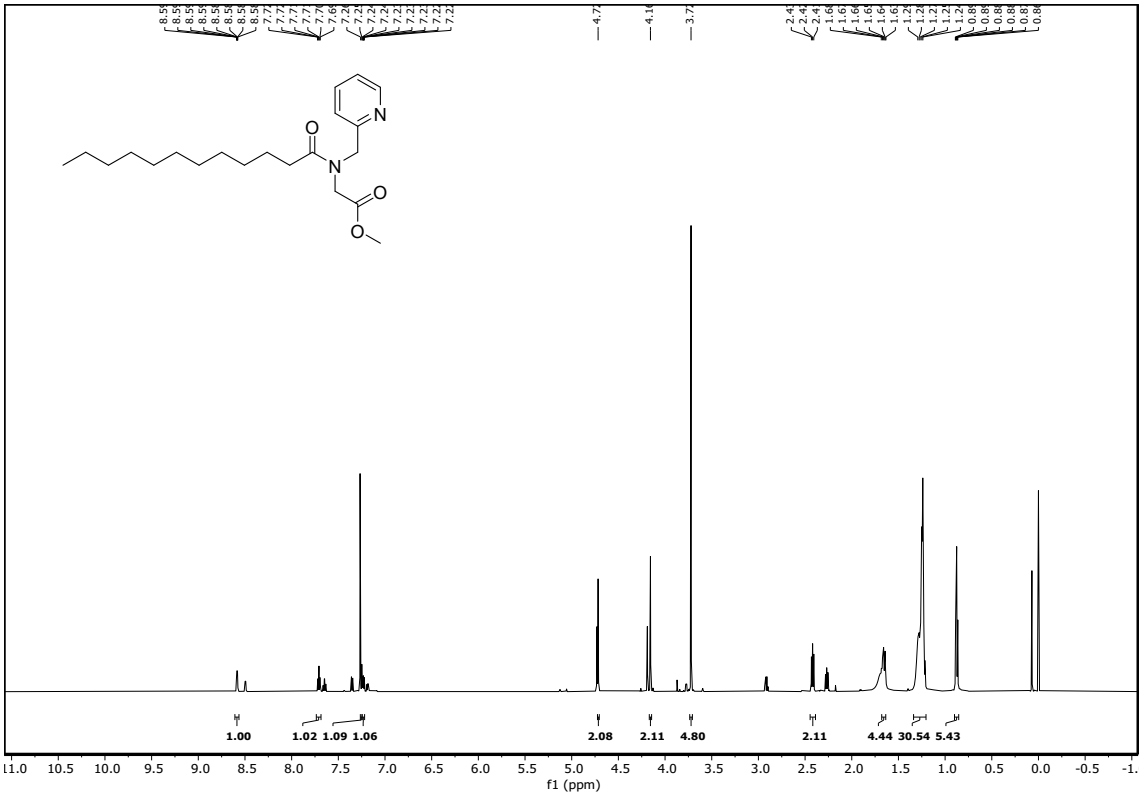

Fig. S3: *N-lauroyl-N-(pyridin-2-ylmethyl)glycine methyl ester (PyN12Ge)*. ^{1}H NMR (600 MHz, $CDCl_3$) δ 8.58 (1H, ddd, *J* = 4.8, 1.8, 1 Hz), 7.71 (1H, td, *J* = 7.8, 1.8 Hz), 7.26 (1H, d, *J* = 7.8 Hz), 7.25 – 7.22 (1H, m), 4.72 (2H, s), 4.16 (2H, s), 3.72 (3H, s), 2.45 – 2.39 (2H, m), 1.68-1.64 (2H, m), 1.34-1.20 (22H, m), 0.88 (3H, td, *J* = 7.2, 1.4 Hz).

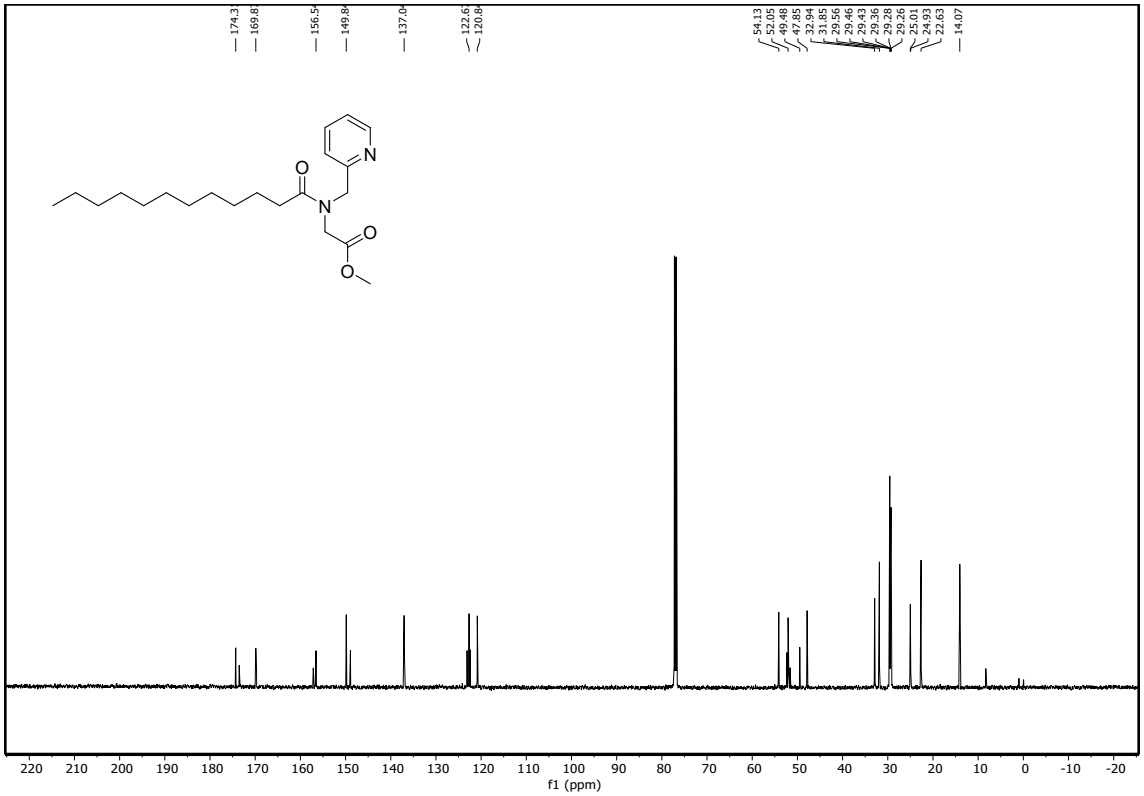

Fig. S4: PyN12Ge ^{13}C NMR (125 MHz). δ 174.31, 169.87, 156.54, 149.84, 137.04, 122.67, 120.84, 54.13, 52.05, 49.48, 47.85, 32.94, 31.85, 29.56, 29.46, 29.43, 29.36, 29.28, 29.26, 25.01, 24.93, 22.63, 14.07.

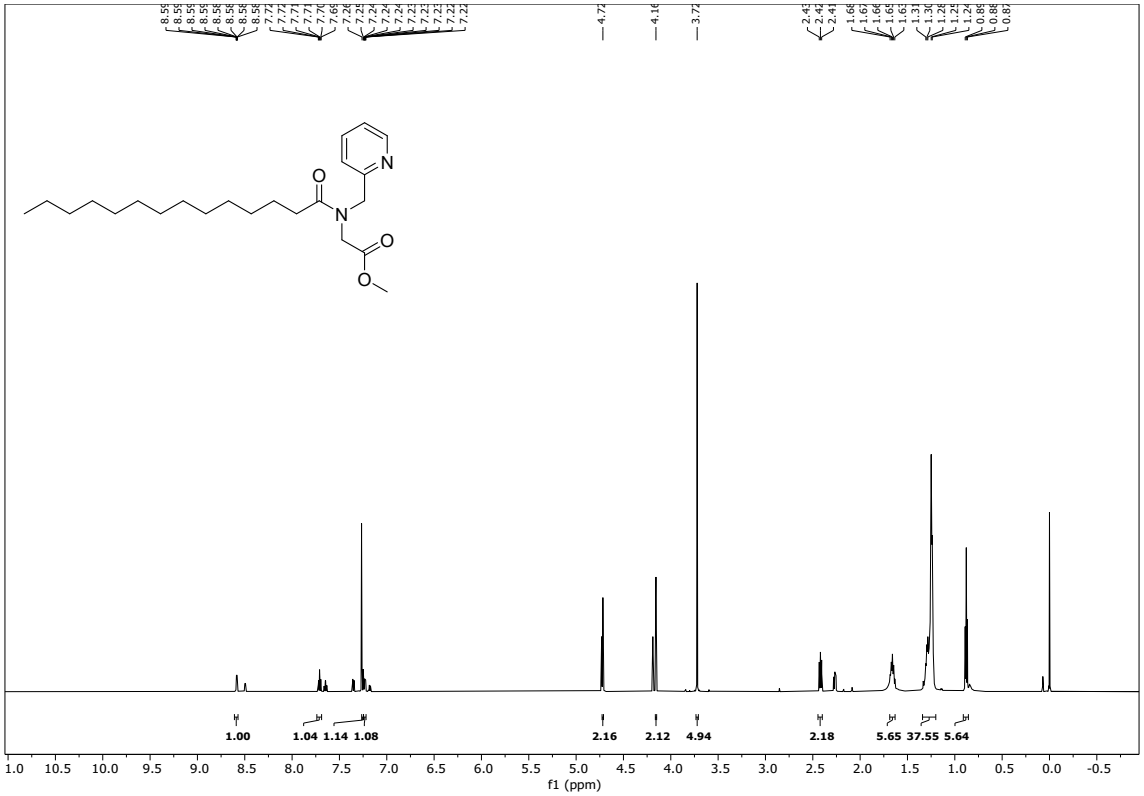

Fig. S5: *N-myristoyl-N-(pyridin-2-ylmethyl)glycine methyl ester (PyN14Ge)*. ^{1}H NMR (600 MHz, $CDCl_3$). δ 8.58 (1H,ddd, *J* = 4.8, 1.8, 1 Hz), 7.71 (1H, td, *J* = 7.8, 1.8 Hz), 7.25 (1H,d, *J* = 7.8 Hz), 7.23 (1H,ddd, *J* = 7.6, 4.8, 1.2 Hz), 4.72 (2H,s), 4.16 (2H,s), 3.72 (3H,s), 2.45 – 2.40 (2H,m), 1.69-1.63 (2H,m), 1.34 – 1.20 (26,m), 0.88 (3H,t, *J* = 7 Hz).

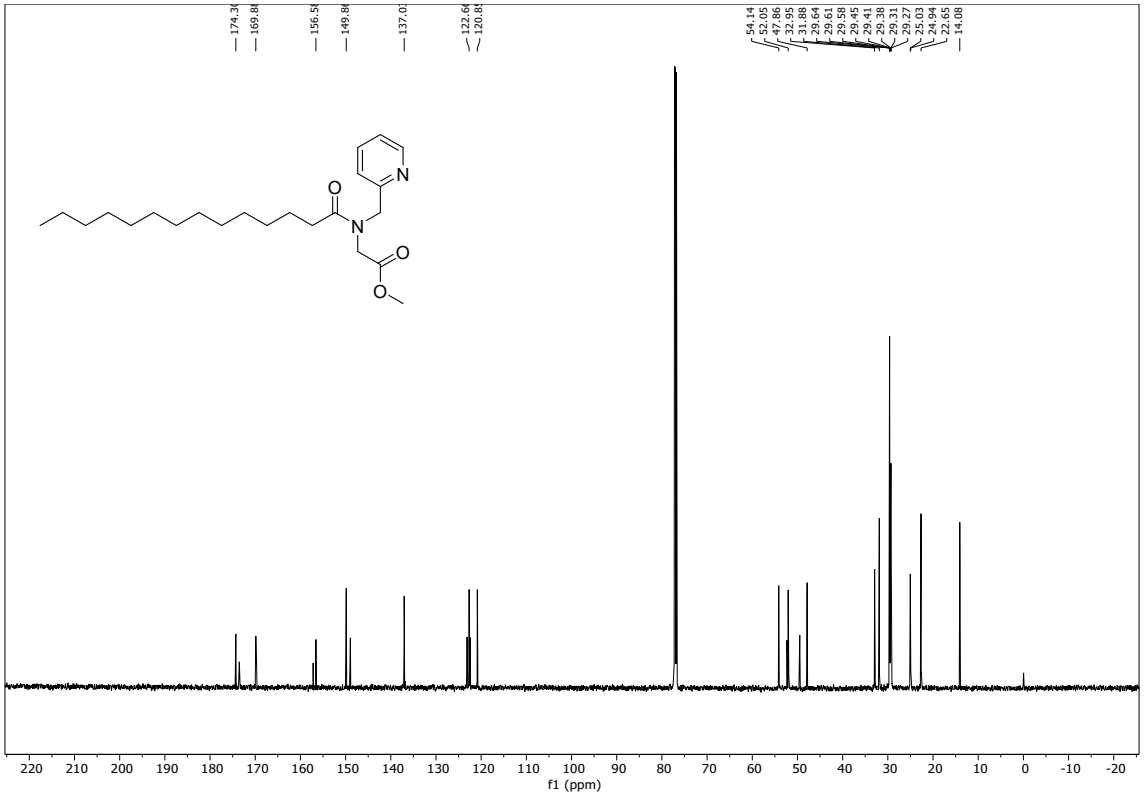

Fig. S6: PyN14Ge ^{13}C NMR (125 MHz). δ 174.30, 169.88, 156.58, 149.86, 137.03, 122.66, 120.85, 54.14, 52.05, 47.86, 32.95, 31.88, 29.64, 29.61, 29.58, 29.45, 29.41, 29.38, 29.31, 29.27, 25.03, 24.94, 22.65, 14.08.

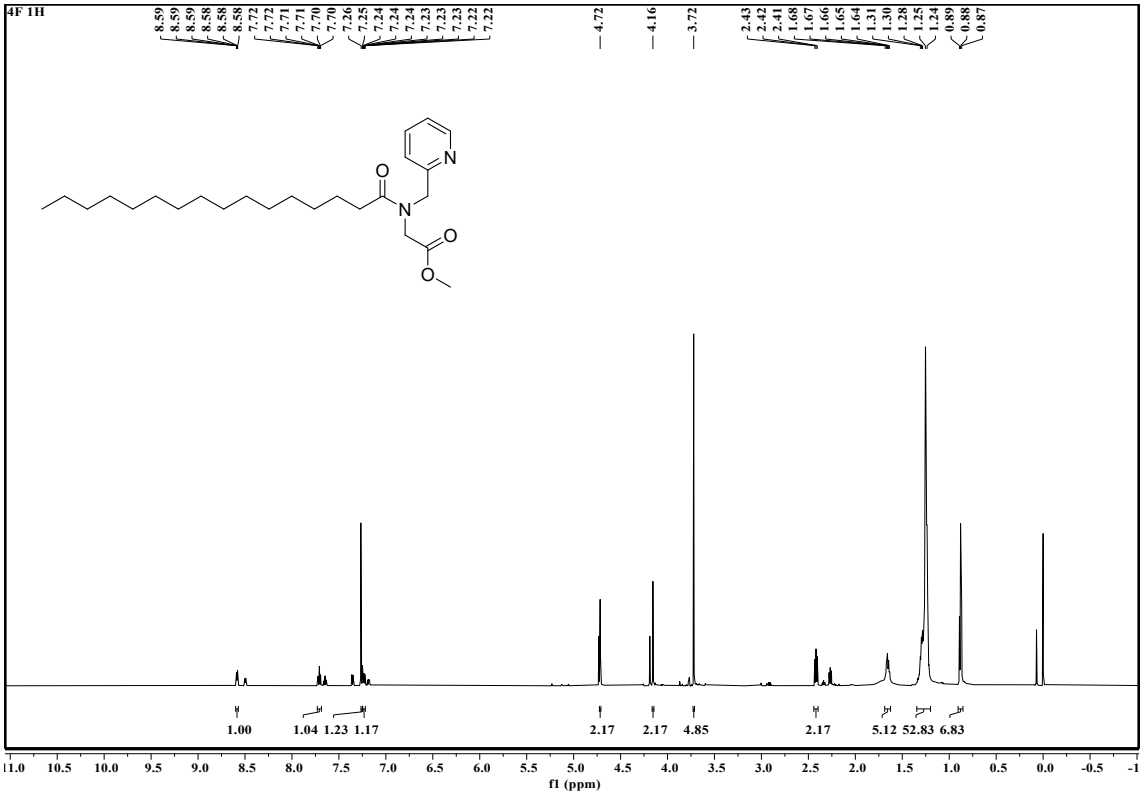

Fig. S7: *N-palmitoyl-N-(pyridin-2-ylmethyl)glycine methyl ester (PyN16Ge)*. ^{1}H NMR (600 MHz, $CDCl_3$). δ 8.58 (1H,dt, *J* = 4.8, 1.4 Hz), 7.71 (1H,td, *J* = 7.6, 1.8 Hz), 7.26 (1H,d, *J* = 7.8 Hz), 7.23 (1H, ddd, *J* = 7.8, 4.8, 1.2 Hz), 4.72 (2H,s), 4.16 (2H,s), 3.72 (3H,s), 2.44 – 2.40 (2H,m), 1.69 – 1.63 (2H,m), 1.35 – 1.20 (30H,m), 0.88 (3H,t, *J* = 7 Hz).

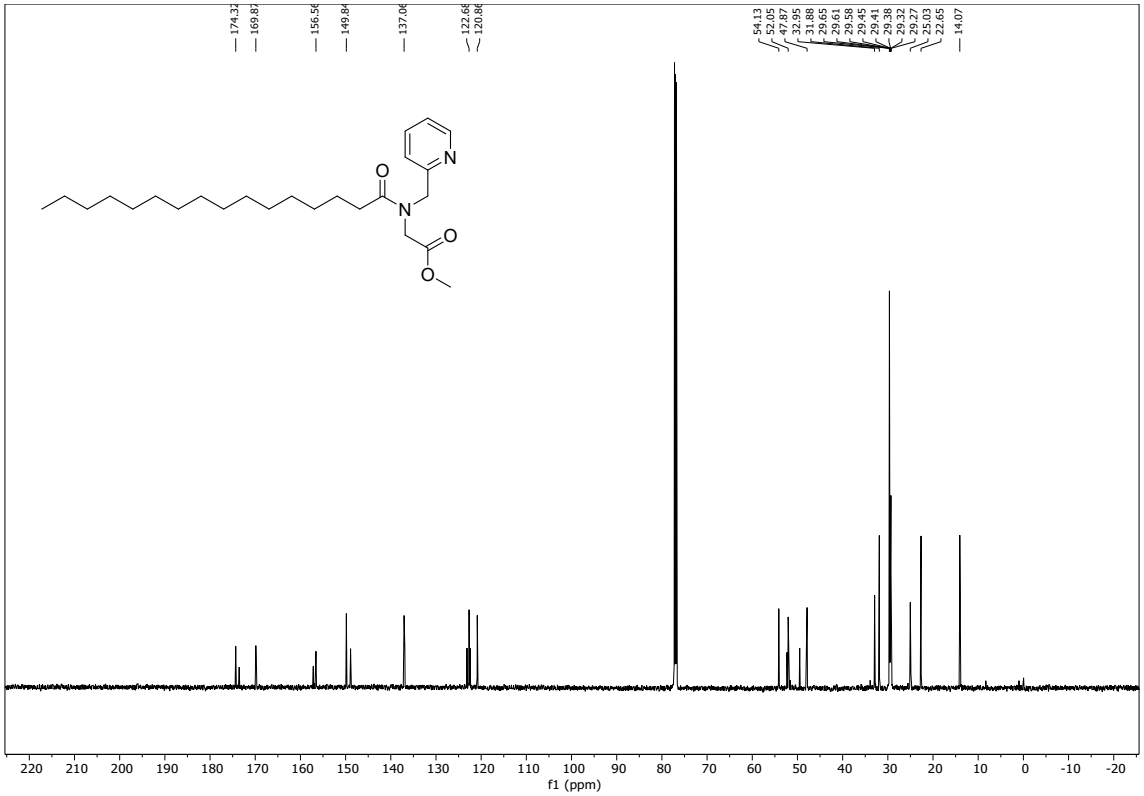

Fig. S8: PyN16Ge ^{13}C NMR (125 MHz). δ 174.32, 169.87, 156.56, 149.84, 137.06, 122.68, 120.86, 54.13, 52.05, 47.87, 32.95, 31.88, 29.65, 29.61, 29.58, 29.45, 29.41, 29.38, 29.32, 29.27, 25.03, 22.65, 14.07.

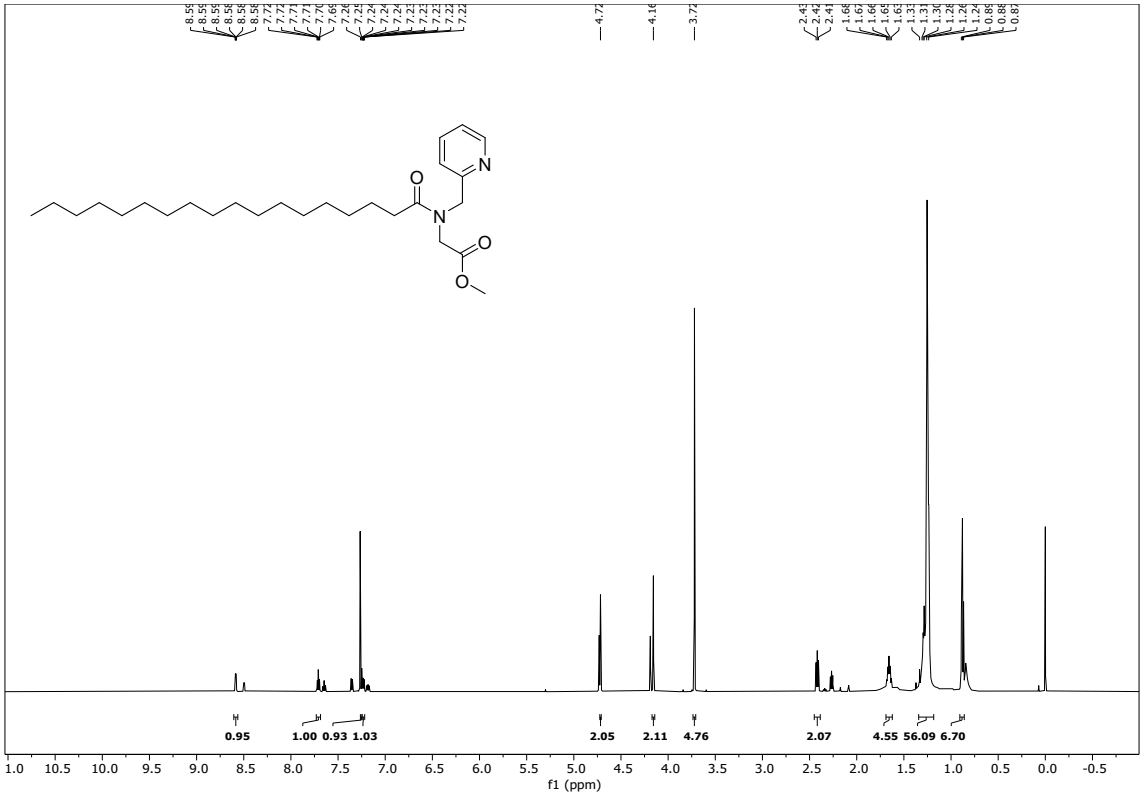

Fig. S9: *N-stearoyl-N-(pyridin-2-ylmethyl)glycine methyl ester (PyN18Ge)*. ^{1}H NMR (600 MHz, $CDCl_3$). δ 8.58 (1H,dt, *J* = 4.8, 1.4 Hz), 7.71 (1H, td, *J* = 7.8, 1.8 Hz), 7.26 (1H, d, *J* = 7.8 Hz), 7.23 (1H, ddd, *J* = 7.8, 4.8, 1.2 Hz), 4.72 (2H,s), 4.16 (2H,s), 3.72 (3H,s), 2.45 – 2.39 (2H, m), 1.69-1.62 (2H, m)), 1.34 – 1.18 (34, m), 0.88 (3H,t, *J* = 3.5 Hz).

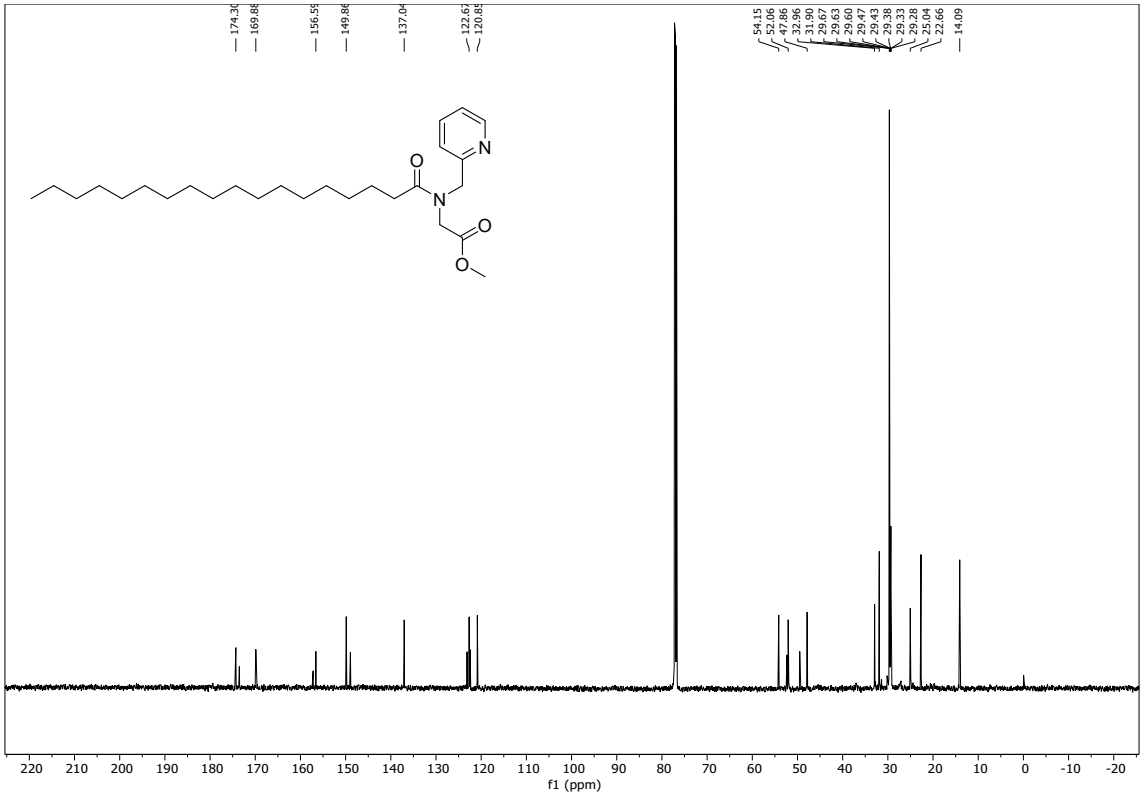

Fig. S10: PyN18Ge ^{13}C NMR (125 MHz). δ 174.30, 169.88, 156.59, 149.86, 137.04, 122.67, 120.85, 54.15, 52.06, 47.86, 32.96, 31.90, 29.67, 29.63, 29.60, 29.47, 29.43, 29.38, 29.33, 29.28, 25.04, 22.66, 14.09.

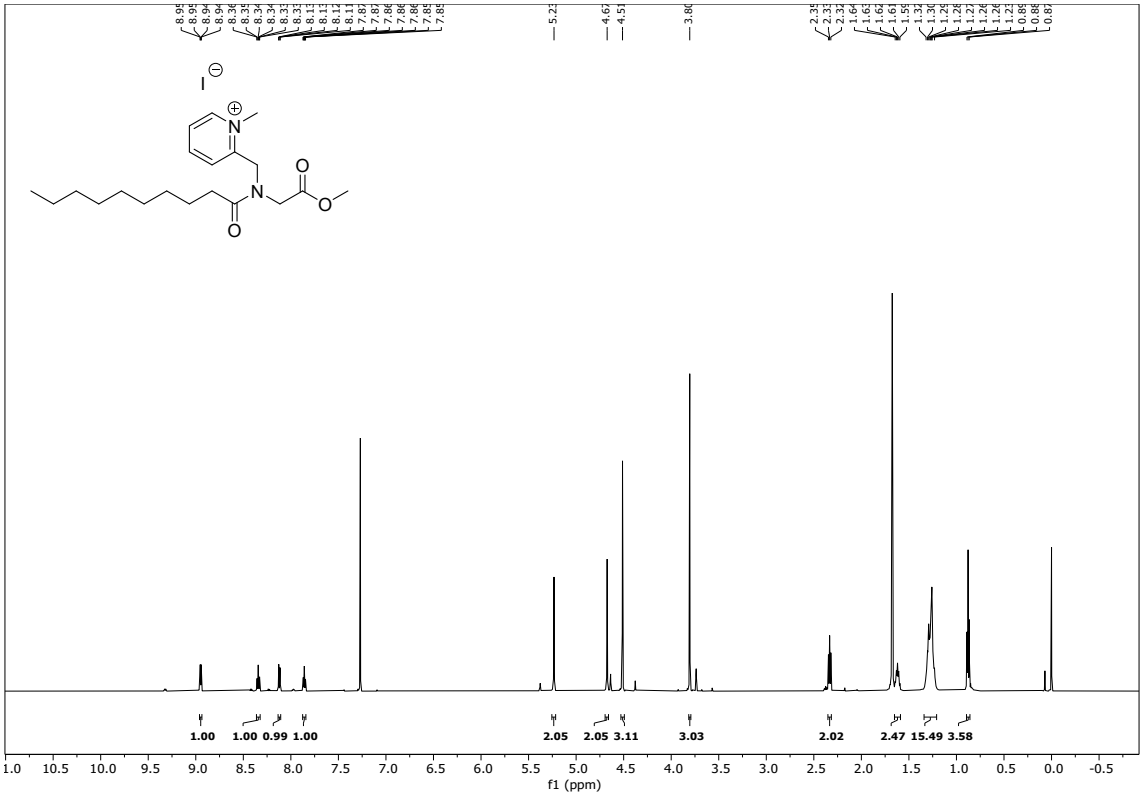

Fig. S11: *2-((N-(2-methoxy-2-oxoethyl)decanamido)methyl)-1-methylpyridin-1-ium (QPyN10Ge)*. ^{1}H NMR (600 MHz, $CDCl_3$). δ 8.95 (1H, dd, *J* = 6.2, 1.6 Hz), 8.34 (1H, td, *J* = 7.8, 1.6 Hz), 8.12 (1H, dd, *J* = 8.2, 1.6 Hz), 7.86 (1H, ddd, *J* = 7.8, 6.0, 1.6 Hz), 5.23 (2H, s), 4.67(2H, s), 4.51 (3H,s), 3.80 (3H,s),, 2.33 (2H, t, *J* = 7.6 Hz), 1.62 (2H, p, *J* = 7.6 Hz), 1.34 – 1.21 (14H, m), 0.88 (3H, t, *J* = 7.0 Hz).

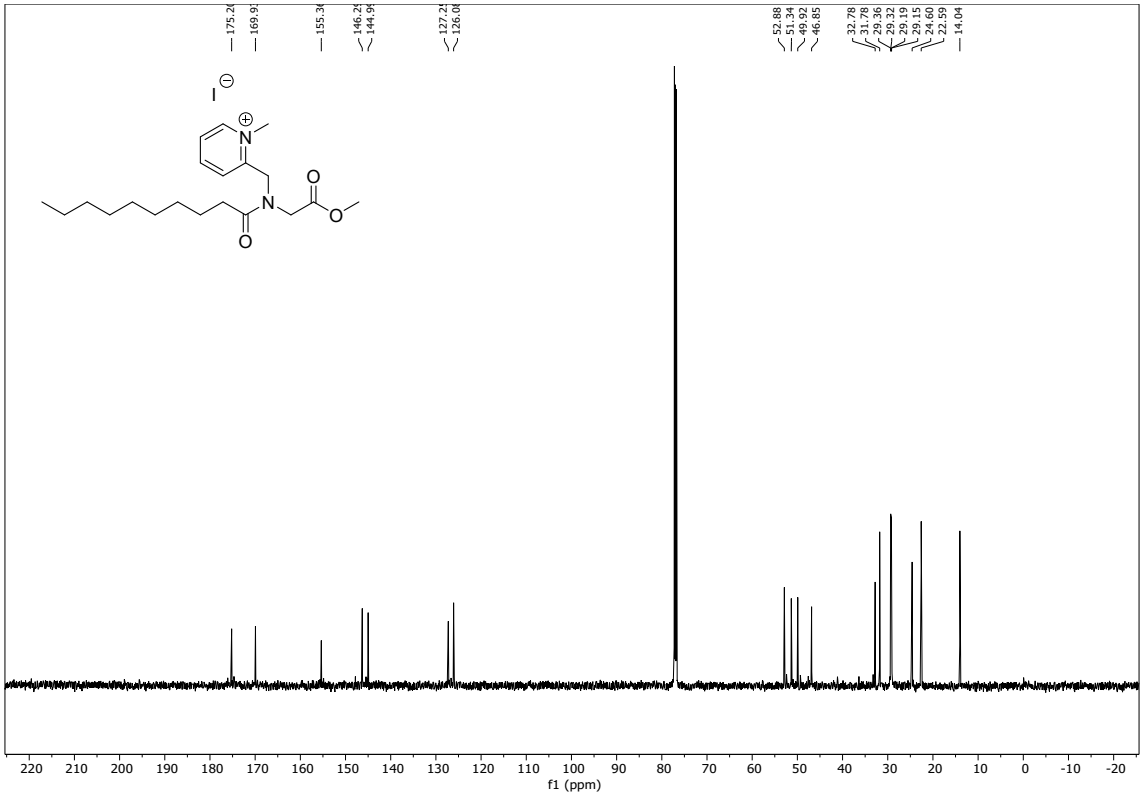

Fig. S12: QPyN10Ge ^{13}C NMR (125 MHz). δ 175.20, 169.93, 155.36, 146.29, 144.99, 127.25, 126.08, 52.88, 51.34, 49.92, 46.85, 32.78, 31.78, 29.36, 29.32, 29.19, 29.15, 24.60, 22.59, 14.04.

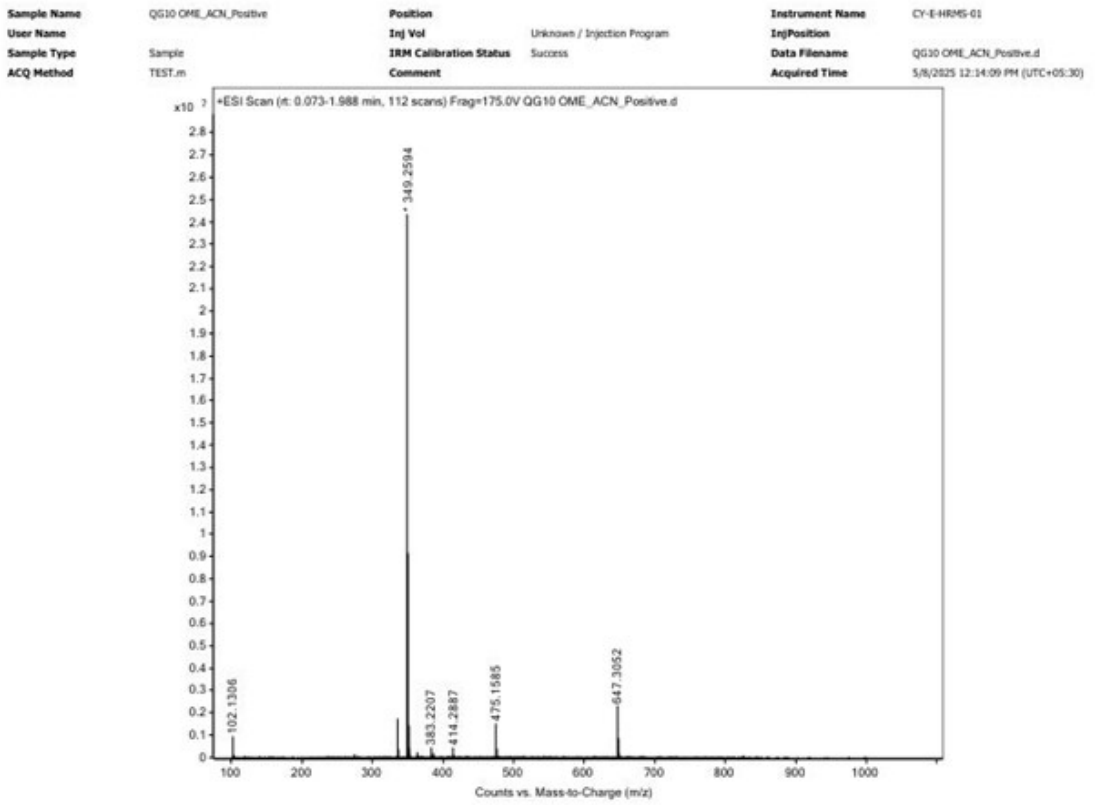

Fig. S13: HRMS of QPyN10Ge. Calculated - 349.49 Found - 349.2594 (M)

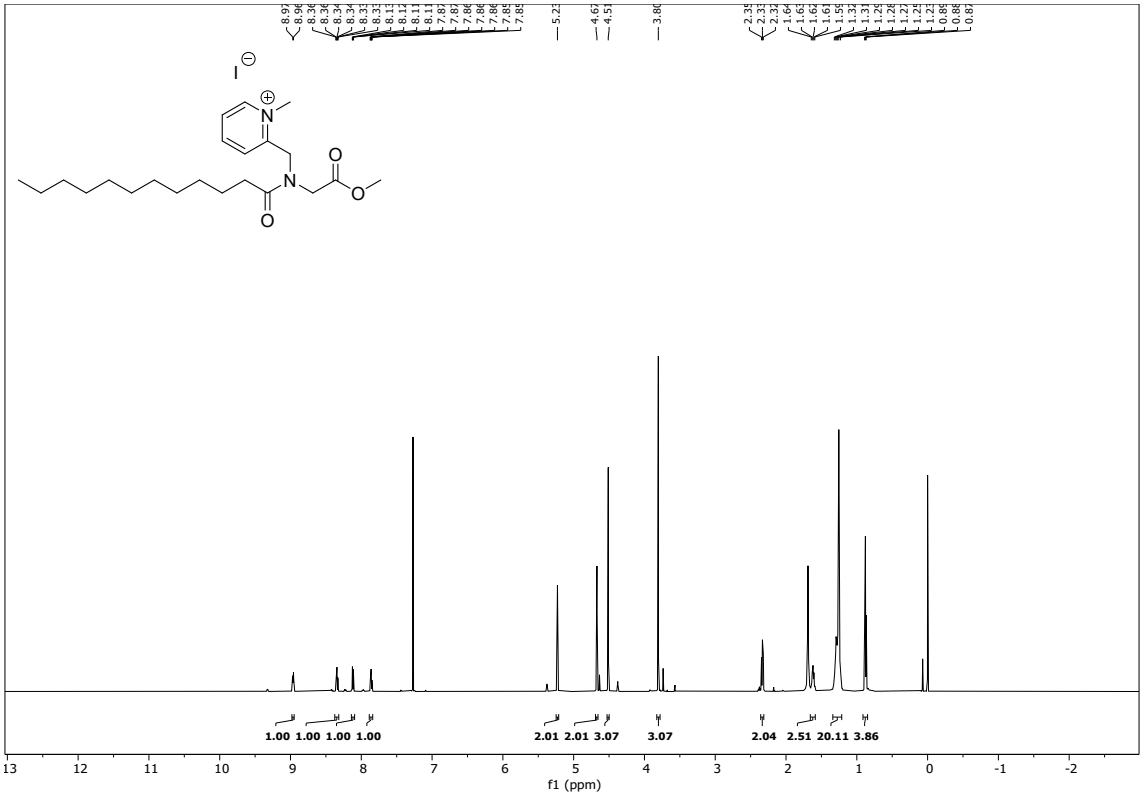

Fig. S14: *2-((N-(2-methoxy-2-oxoethyl)dodecanamido)methyl)-1-methylpyridin-1-ium (QPyN12Ge)*. ^{1}H NMR (600 MHz, $CDCl_3$). δ 8.96 (1H, d, *J* = 6.4 Hz), 8.34 (1H, td, *J* = 8.0, 1.6 Hz), 8.12 (1H, dd, *J* = 8.2, 1.6 Hz), 7.86 (1H, ddd, *J* = 7.8, 6.0, 1.6 Hz), 5.23 (2H,s), 4.67 (2H,s), 4.51 (3H,s), 3.80 (3H,s), 2.33 (2H,t, *J* = 7.6 Hz),, 1.62 (2H, p, *J* = 7.6 Hz), 1.34 – 1.21 (18H, m), 0.88 (3H, t, *J* = 7.0 Hz).

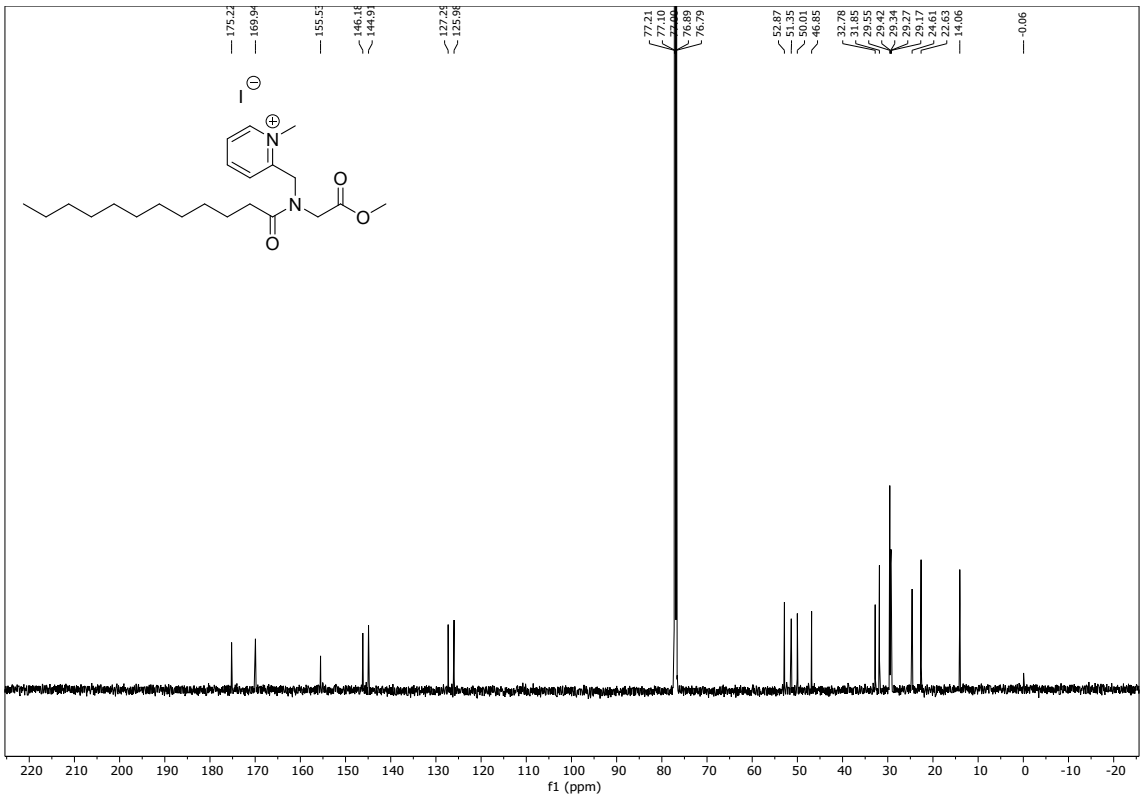

Fig. S15: QPyN12Ge ^{13}C NMR (125 MHz). δ 175.22, 169.94, 155.53, 146.18, 144.91, 127.29, 125.98, 52.87, 51.35, 50.01, 46.85, 32.78, 31.85, 29.55, 29.42, 29.34, 29.27, 29.17, 24.61, 22.63, 14.06.

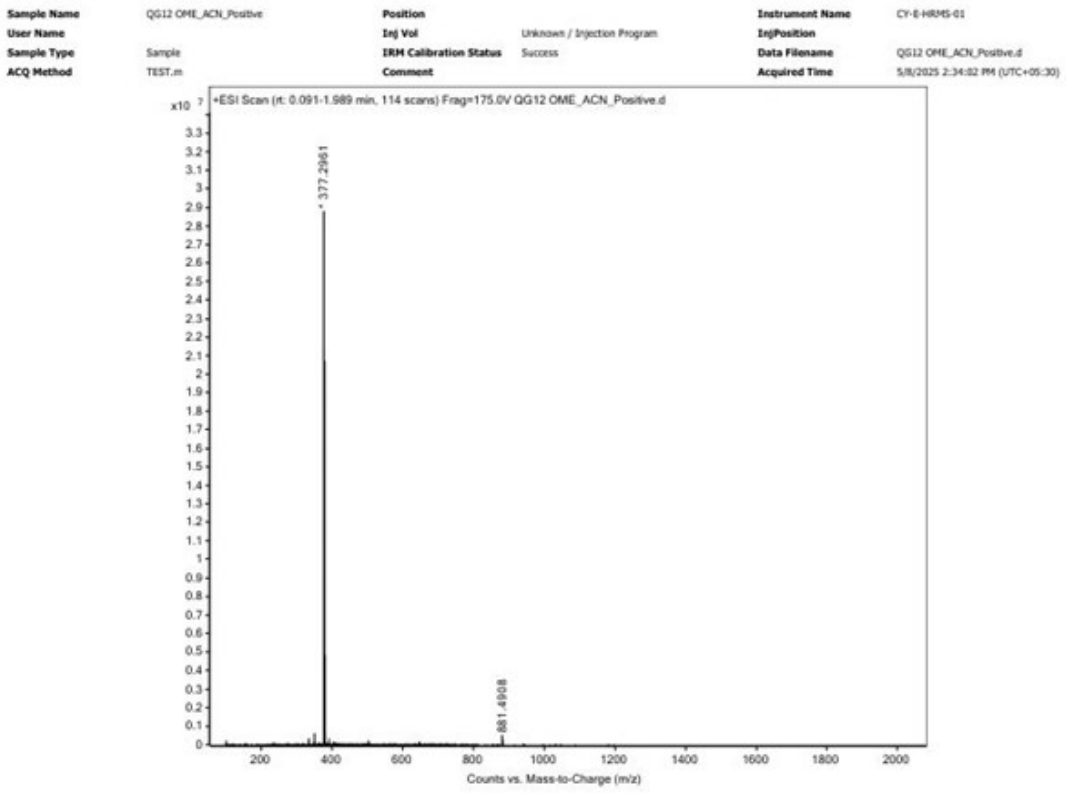

Fig. S16: HRMS of PyN12Ge, Calculated - 377.55, Found - 377.2961 (M)

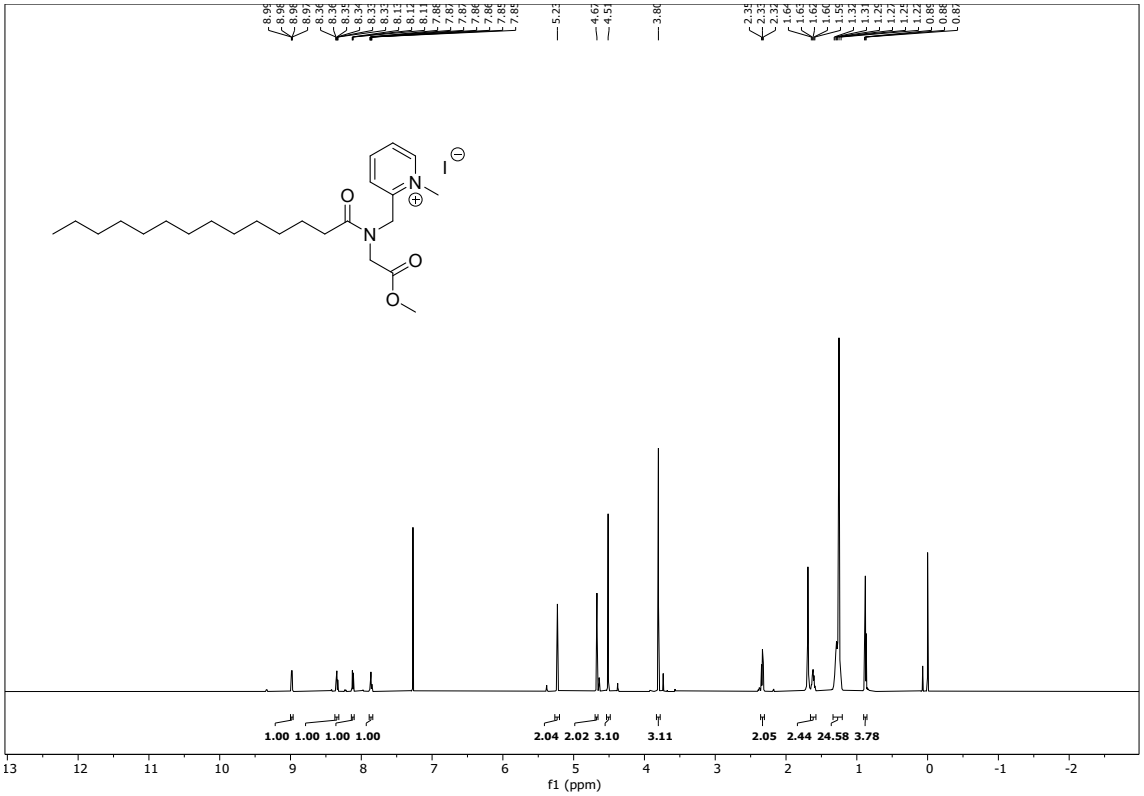

Fig. S17: *2-((N-(2-methoxy-2-oxoethyl)tetracanamido)methyl)-1-methylpyridin-1-ium (QPyN14Ge).* δ 8.98 (1H,dd, *J* = 6.2, 1.6 Hz), 8.34 (1H,td, *J* = 7.8, 1.6 Hz), 8.12 (1H,dd, *J* = 8.2, 1.6 Hz), 7.86 (1H,ddd, *J* = 7.8, 6.2, 1.6 Hz), 5.23 (2H,s), 4.67 (2H,s), 4.51 (3H,s), 3.80 (3H,s) 2.33 (2H,t, *J* = 7.6 Hz), 1.62 (2H, p, *J* =7.6 Hz), 1.34-1.21 (22H,m), 0.88 (3H,t, *J* = 7 Hz).

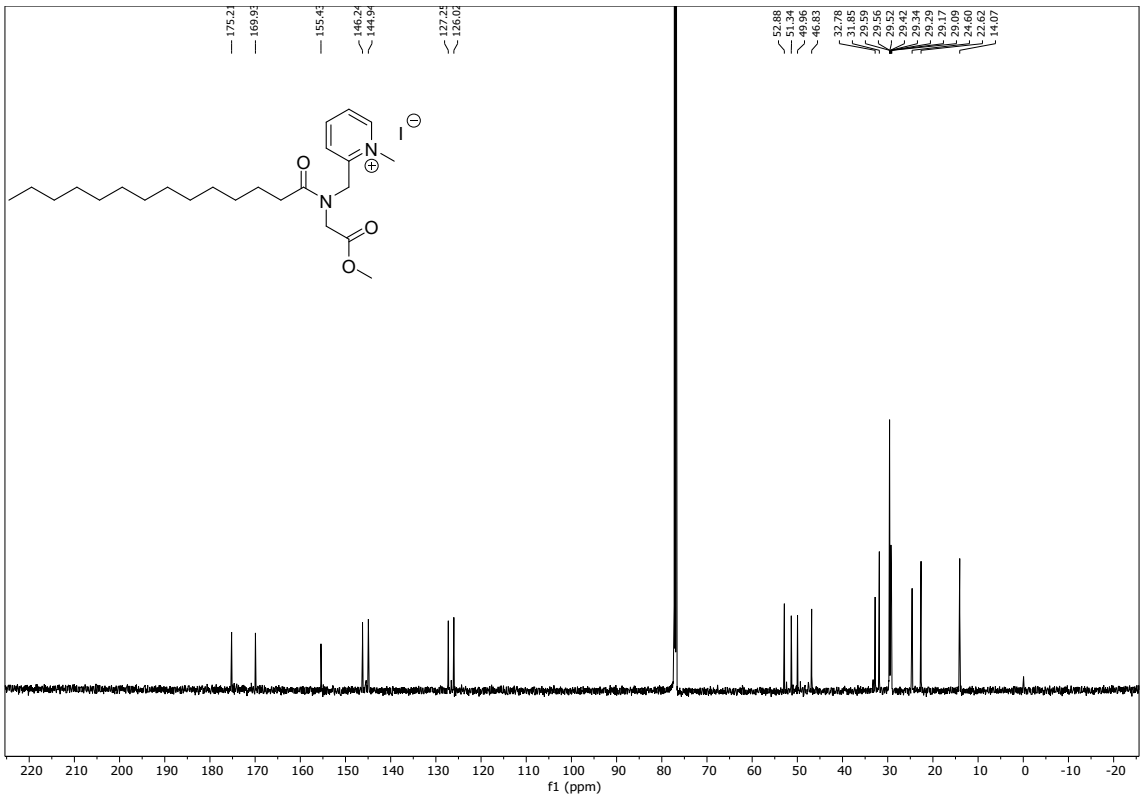

Fig. S18: QPyN14Ge ^{13}C NMR (125 MHz). δ 175.21, 169.93, 155.43, 146.24, 144.94, 127.25, 126.02, 52.88, 51.34, 49.96, 46.83, 32.78, 31.85, 29.59, 29.56, 29.52, 29.42, 29.34, 29.29, 29.17, 29.09, 24.60, 22.62, 14.07.

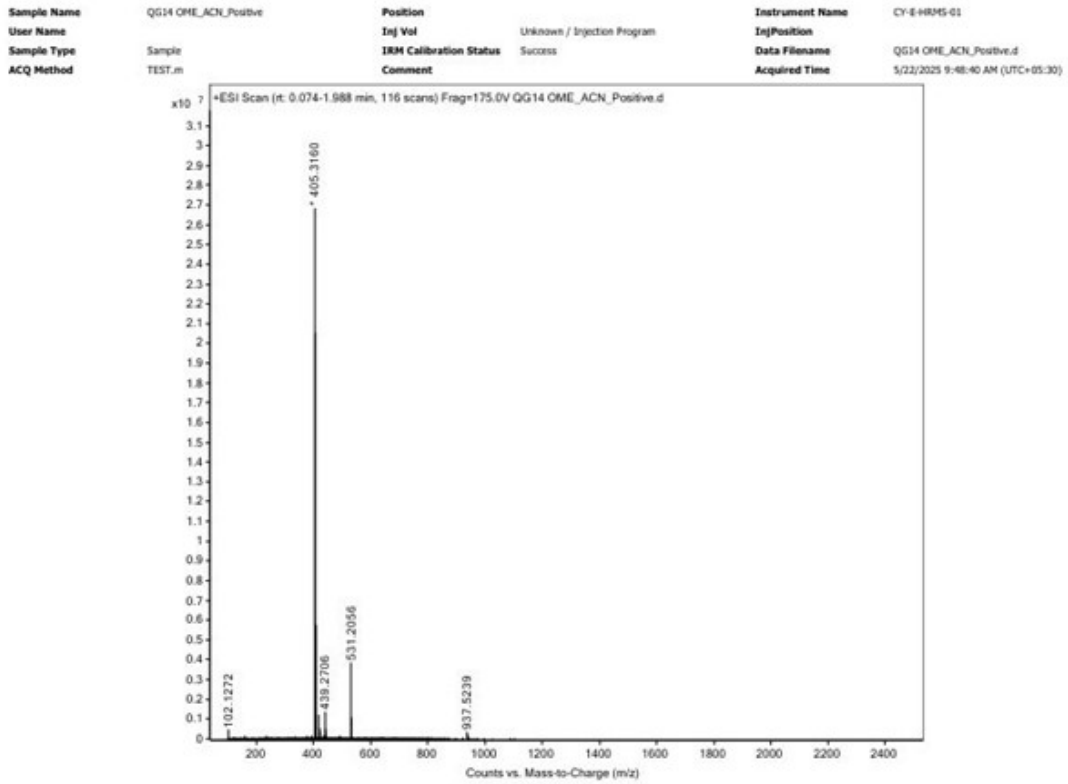

Fig. S19: HRMS of QPyN14Ge, Calculated - 405.60, Found - 405.3160 (M)

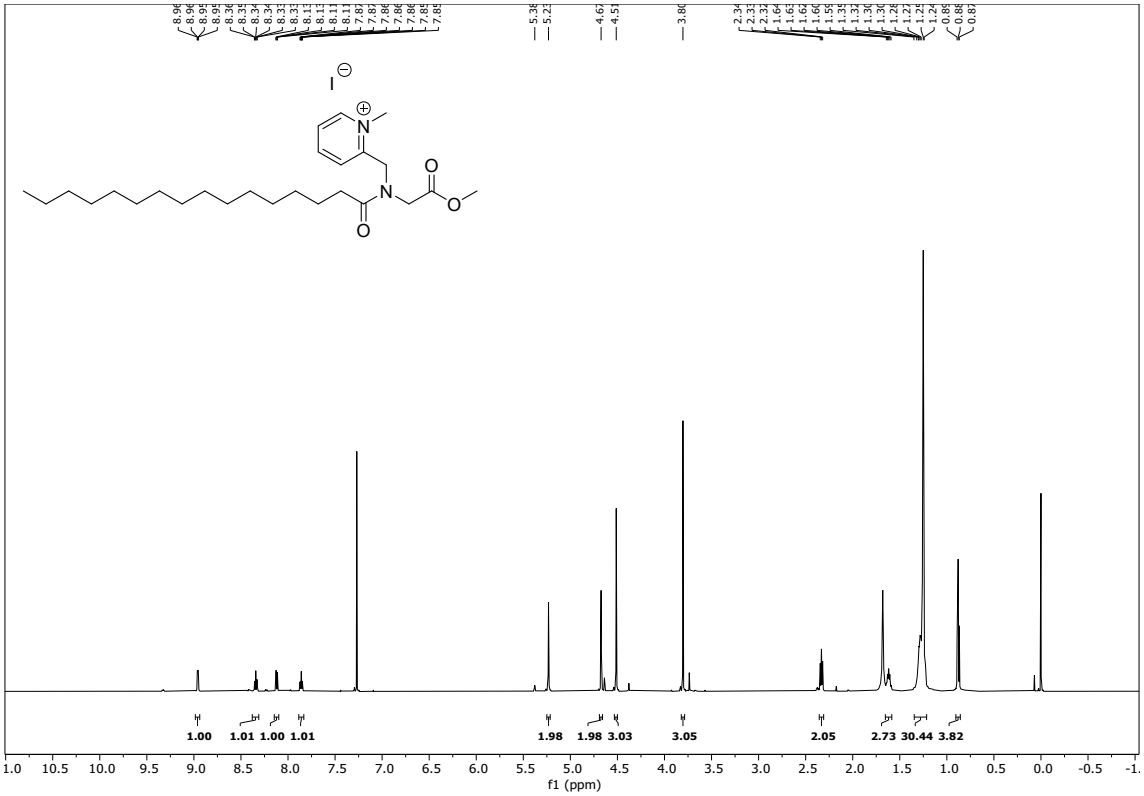

Fig. S20: *2-((N-(2-methoxy-2-oxoethyl)palmitamido)methyl)-1-methylpyridin-1-ium (QPyN16Ge).* ^{1}H NMR (600 MHz, $CDCl_3$). δ 8.96 (1H, dd, *J* = 6.2, 1.6 Hz), 8.34 (1H, td, *J* = 8.0, 1.6 Hz), 8.12 (1H, dd, *J* = 8.2, 1.6 Hz), 7.86 (1H, ddd, *J* = 7.8, 6.0, 1.6 Hz), 5.23 (2H,s), 4.67(2H,s), 4.51 (3H,s), 3.80 (3H,s), 2.33 (2H, t, *J* = 7.6 Hz), 1.62 (2H, p, *J* = 7.6 Hz), 1.35-1.21 (26H,m), 0.88 (3H,t, *J* = 7 Hz).

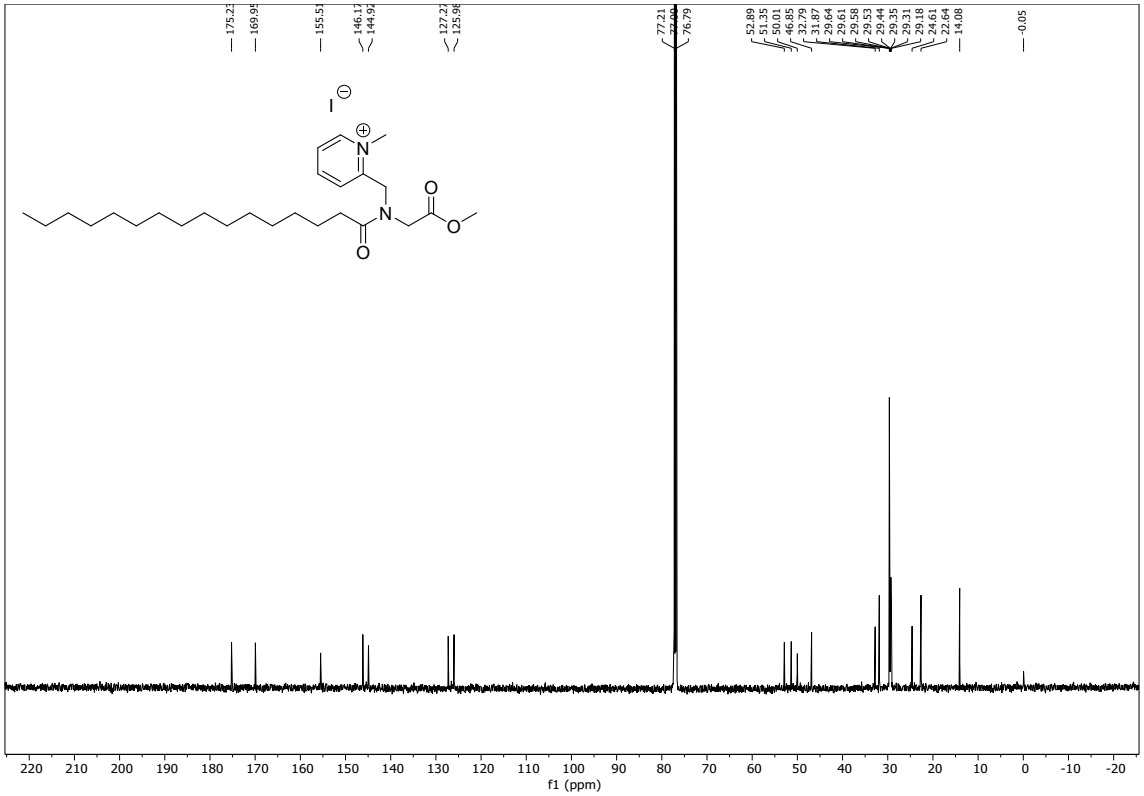

Fig. S21: QPyN16Ge ^{13}C NMR (125 MHz). δ 175.23, 169.95, 155.51, 146.17, 144.92, 127.27, 125.98, 52.89, 51.35, 50.01, 46.85, 32.79, 31.87, 29.64, 29.61, 29.58, 29.53, 29.44, 29.35, 29.31, 29.18, 24.61, 22.64, 14.08.

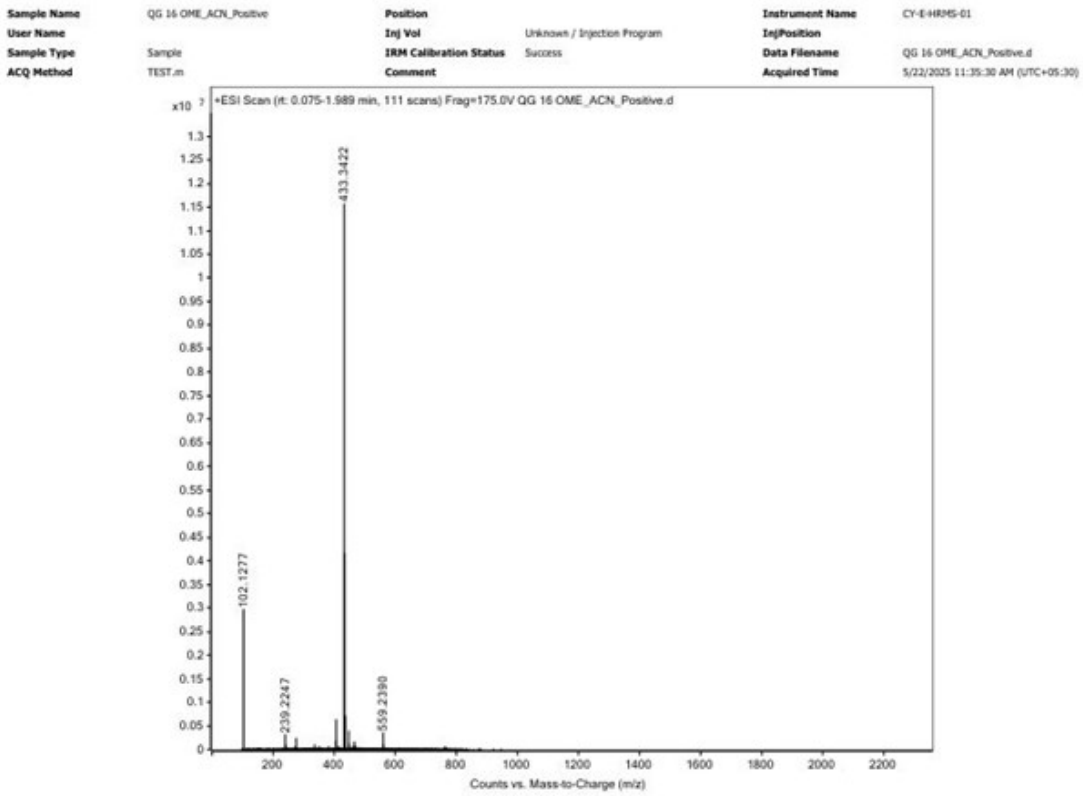

Fig. S22: HRMS of QPyN16Ge, Calculated - 433.66 Found - 433.3422 (M)

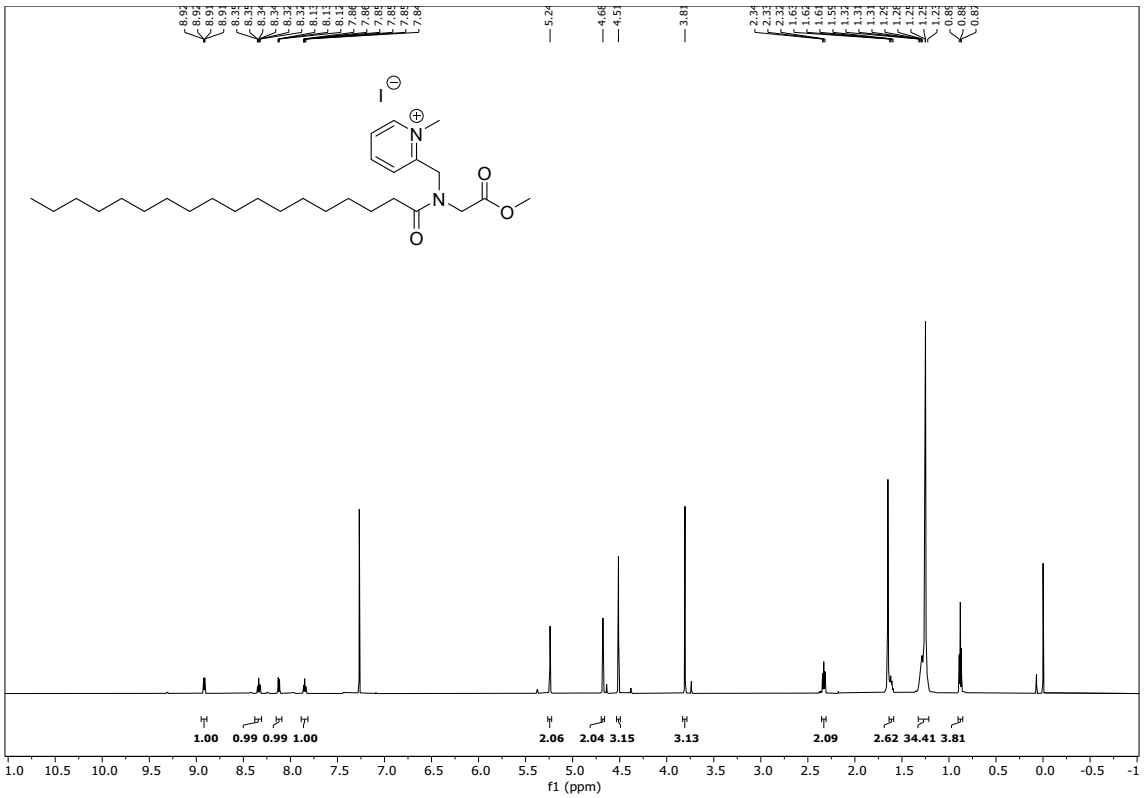

Fig. S23: *2-((N-(2-methoxy-2-oxoethyl)stearamido)methyl)-1-methylpyridin-1-ium (QPyN18Ge).* ^{1}H NMR (600 MHz, $CDCl_3$). δ 8.92 (1H, dd, *J* = 6.2, 1.4 Hz), 8.34 (1H, td, *J* = 8.0, 1.6 Hz), 8.15 – 8.09 (1H, m), 7.89 – 7.81 (1H, m), 5.24 (2H,s), 4.68 (2H,s), 4.51 (3H,s) 3.81 (3H,s),, 2.33 (2H,t, *J* = 7.6 Hz), 1.64-1.58 (2H, m), 1.33-1.21 (30H, m), 0.88 (3H, t, *J* = 7 Hz).

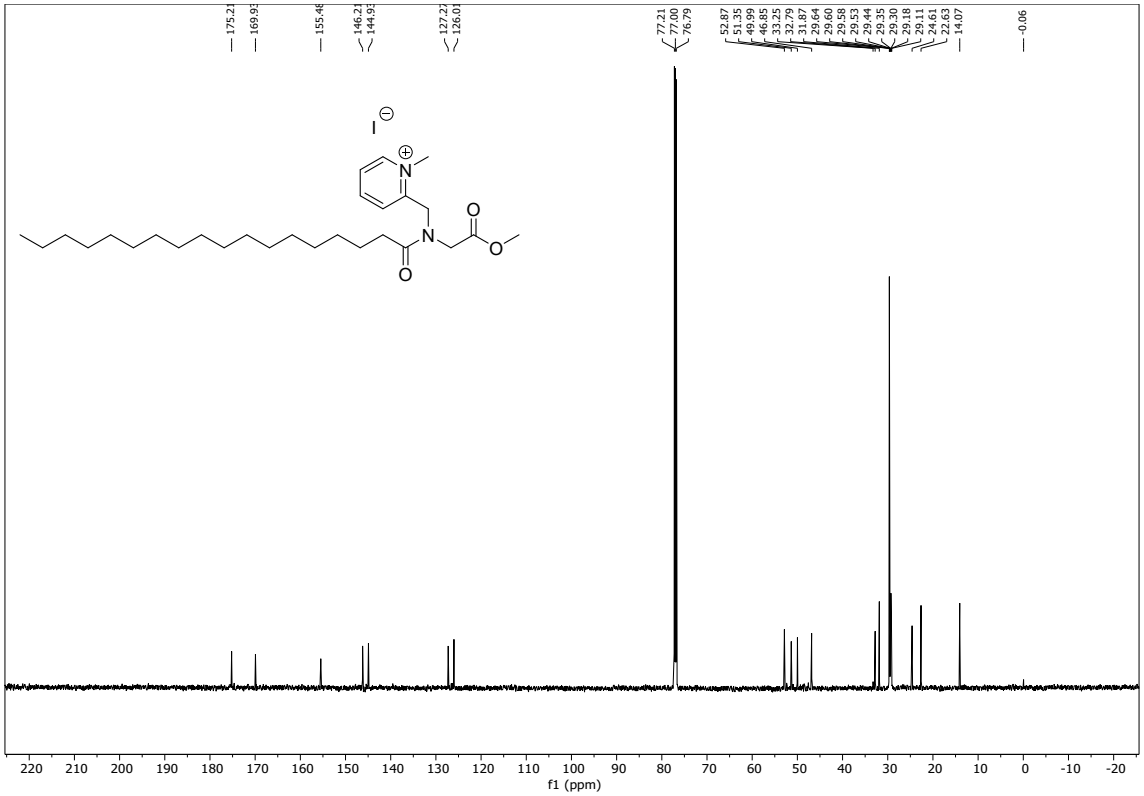

Fig. S24: QPyN18Ge ^{13}C NMR (125 MHz). δ 175.21, 169.93, 155.48, 146.21, 144.93, 127.27, 126.01, 52.87, 51.35, 49.99, 46.85, 33.25, 32.79, 31.87, 29.64, 29.60, 29.58, 29.53, 29.44, 29.35, 29.30, 29.18, 29.11, 24.61, 22.63, 14.07.

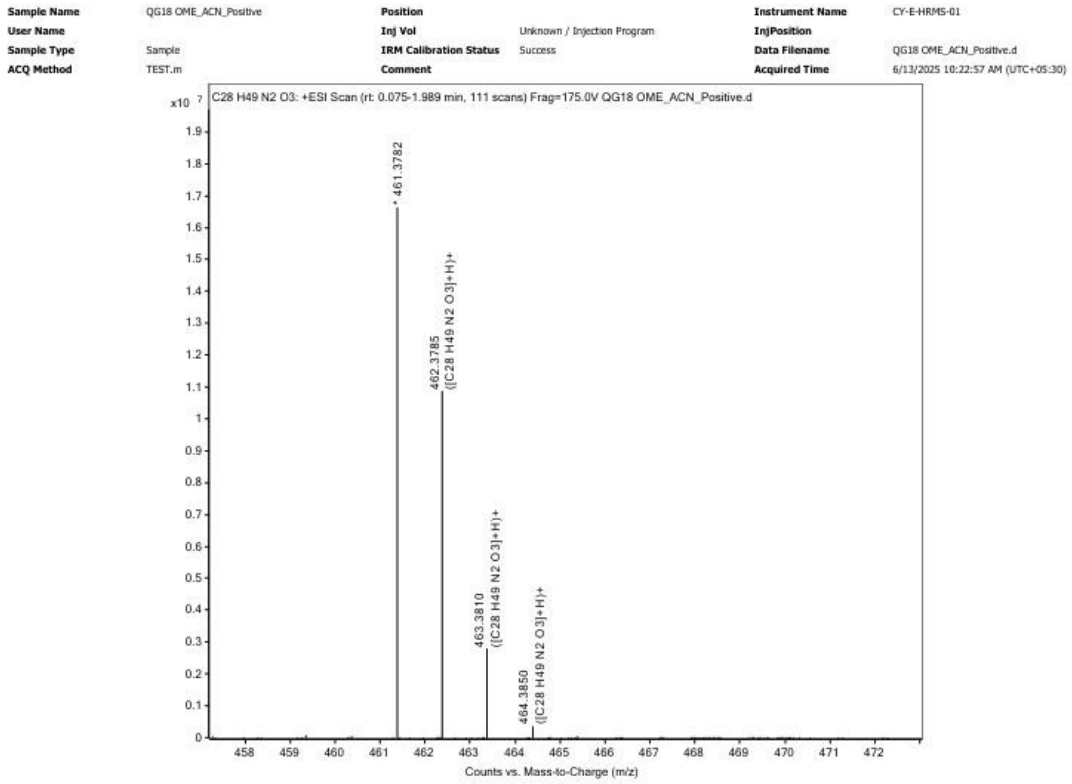

Fig. S25: HRMS of QPyN18Ge, Calculated- 461.71 Found- 461.3782 (M)

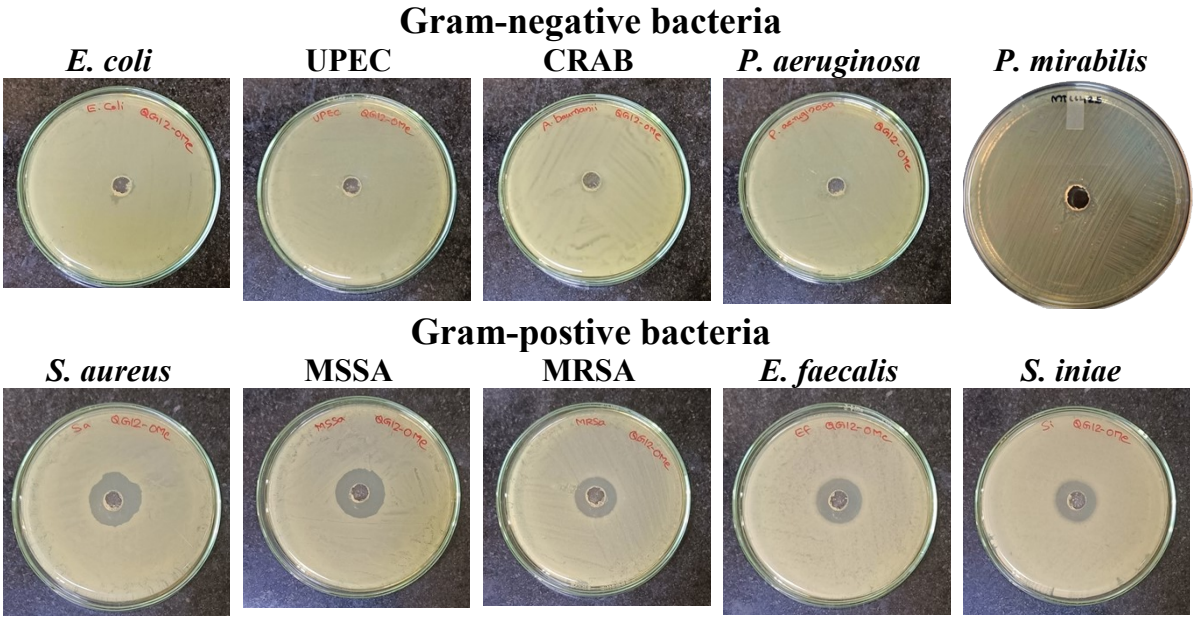

Fig. S26: Zone of Inhibition assay.

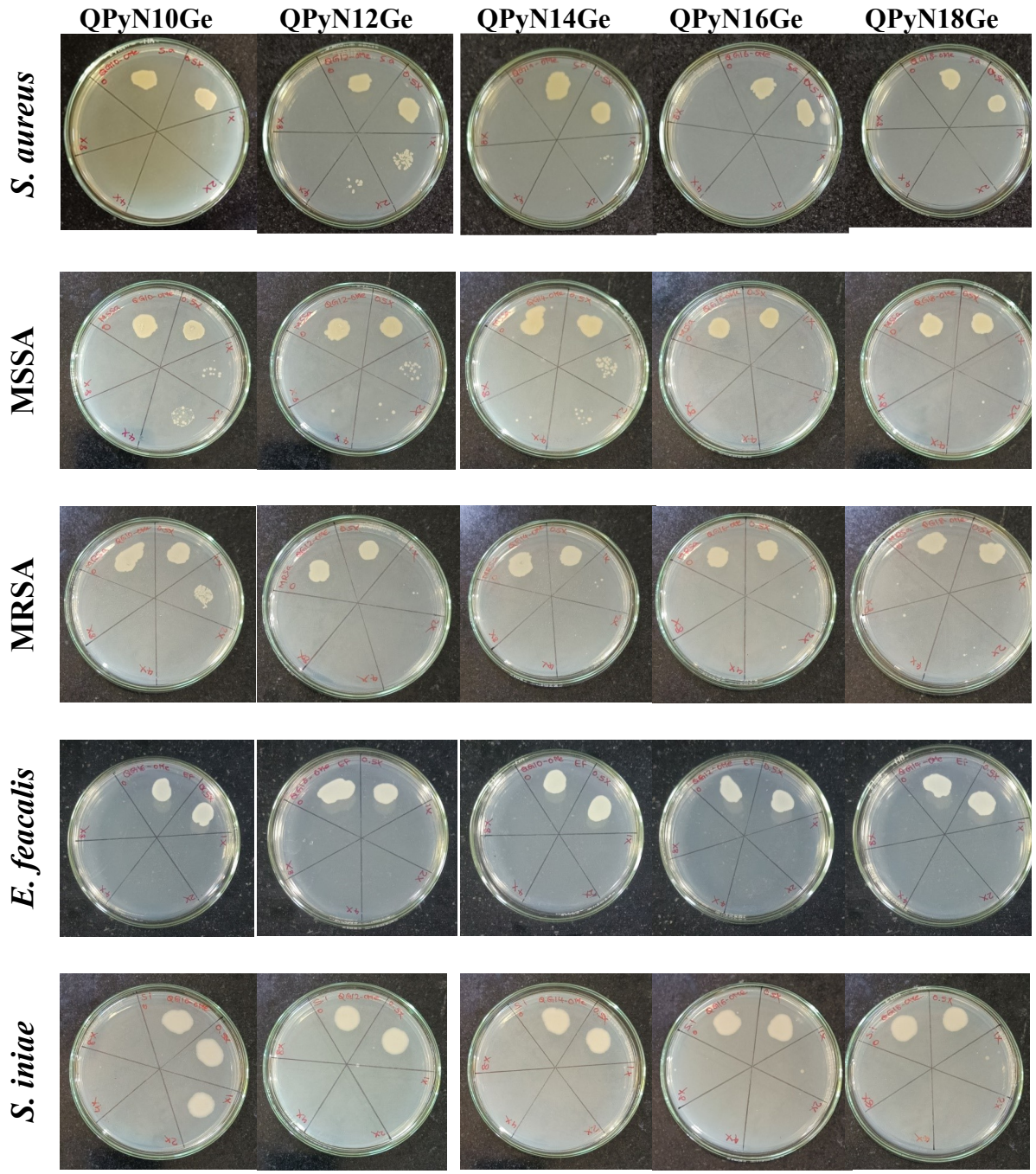

Fig. S27: Determination of minimum bactericidal concentration

Table S1: MBC determined by spot test and HL/MBC ratio was presented to show hemocompatibility

Molecule	*S. aureus*		MSSA		MRSA		*S. iniae*		*E. feacalis*	
	MBC	**HLC/ MBC**	**MBC**	**HLC/ MBC**	**MBC**	**HLC/ MBC**	**MBC**	**HLC/ MBC**	**MBC**	**HLC/ MBC**
QPyN10Ge	500	8	2000	2	2000	2	2000	2	1000	4
QPyN12Ge	125	8	250	4	250	4	250	4	125	8
QPyN14Ge	7.81	64	15.63	32	31.25	16	31.25	16	7.81	64
QPyN16Ge	3.91	128	3.91	128	7.81	64	7.81	64	7.81	64
QPyN18Ge	3.91	128	7.81	64	7.81	64	7.81	64	15.63	32

Molecular docking and Molecular dynamics simulation

The three-dimensional crystal structures of *S. aureus* enzymes were retrieved from the Protein Data Bank (https://www.rcsb.org) using their respective PDB IDs: Aminoacyltransferase FemA (1LRZ), Penicillin-binding protein 2 (1MWT), Monofunctional glycosyltransferase (3VMT, 6FTB). The proteins were prepared for molecular docking using the 'Protein Preparation Wizard' in Maestro. Energy minimization was carried out using the OPLS4 force field. The chemical structures of the ligands, QPyN18Me, QPyN16Me, QPyN12Me, QPyN10Me, and QPyN14Me were drawn using Maestro 2D sketcher. The binding site of the prepared proteins was identified using the SiteMap module in Maestro. A receptor grid was generated using 'Receptor Grid Generation' around the predicted binding sites, and the prepared ligands were docked using the Glide extra precision (XP) docking protocol with default parameters. Molecular dynamics (MD) simulations were carried out for both the apo form and the ligand-bound complex using the 'Desmond' module. Production MD simulations were performed for 200 ns for each system using the OPLS4 force field. Trajectories were recorded for post-simulation analysis of structural stability and protein–ligand interactions.

The biophysical investigations presented above clearly demonstrate that QPyNAGe disrupts the bacterial cell wall. The cell wall peptidoglycan is synthesized in various phases, each involving a separate enzyme and protein complex. For instance, the Fem proteins (PDB ID: 1LRZ) play a crucial role in forming the interbridge pentaglycyl chain, which provides the cell wall with structural integrity. Penicillin-binding protein 2a (PDB ID: 1MWT) catalyses the crosslinking of pentaglycine bridges. The glycosyltransferase domain (PDB ID: 3VMT) of *S. aureus* PBP2 catalyses the final polymerization of peptidoglycan and wall teichoic acids, whereas another glycosyltransferase protein (PDB ID: 6FTB) polymerizes the precursor molecule, Lipid II, into lengthy glycan chains. These proteins are currently the subject of drug discovery because inhibiting them prevents cell wall biosynthesis. A molecular docking technique was employed to assess the potential binding of QPyNAGe to the 1LRZ, 1MWT, 3VMT, and 6FTB molecules.

The prepared protein structures and ligands were docked using the generated grid file. The docking score for QPyNAGe in binding with proteins involved in cell biosynthesis is shown in Table S2 (see supporting Table S2). It is noted from Table S2 that QPyNAGe shows preferential binding to the aminoacyltransferase FemA protein (1LRZ). Among the docked complexes, QPyN16Me exhibited the top docking score with 1LRZ, indicating a strong binding affinity. The top-scoring ligand, QPyN16Me, forms key interactions,

including hydrogen bonds with Ile155, Asp150, and Glu213, an ionic interaction with Asp219, and hydrophobic contacts with Val152, Leu153, Gly330, Gly331, and Val379, as observed in 1LRZ. The ligands formed fewer interactions with other targets, resulting in significantly poorer docking scores. In 1MWT, the compound interacts with Asn464 through a hydrogen bond and with Tyr446 through π–π-cation interaction. In 3VMT, QPyN16Me forms an ionic interaction with Arg241, while in 6FTB, it forms a hydrogen bond with Asn141 and an ionic bond with Asp145. Among all targets, a greater number of stabilizing interactions were observed in the 1LRZ–QPyN16Me complex, which correlated with its higher affinity. It is noted from the 3D ligand interaction diagram (Fig. S28A) that the ligand forms an interaction network with both catalytic and its neighboring residues, particularly those involved in the previously reported active function of FemA Transferase pocket residues: Arg220, Phe224, and Tyr327.

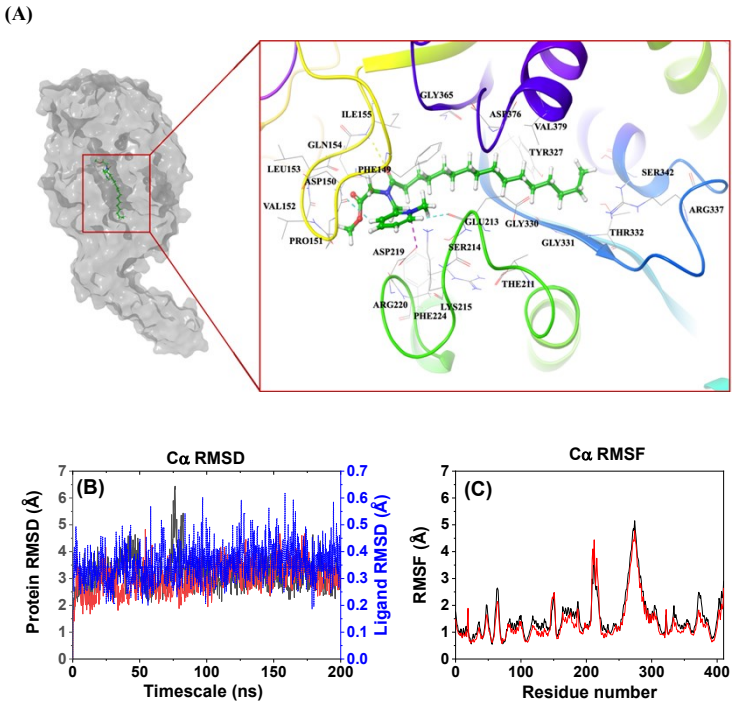

Fig. S28: (A) 3D ligand–protein interaction diagram of compound QPyN16Ge with the FemA protein, PDB ID – 1LRZ. Key interactions, includes hydrogen bonds with Ile155, Asp150, and Glu213, an ionic interaction with Asp219, and hydrophobic contacts with Val152, Leu153, Gly330, Gly331, and Val379. (B) Molecular dynamics simulation. (B) Root Mean Square Deviation (RMSD). Blue line is ligand RMSD.and (C) Root Mean Square Fluctuation (RMSF) between FemA (black line) and FemA-QPyN16Ge bound form (red line).

The MD simulations were performed on the apo form of FemA and its complex with QPyN16Ge for 200 ns. The root mean square plots suggest that both the apo and complex forms are generally stable (Cα RMSD range 2.0–4.0 Å), and the stability of the ligand-bound form is increased (Fig. S28B). The RMSD of ligand is stable throughout the dynamic simulation. The RMSF data for the ligand-bound state indicate that the regions correlating with residues 180–188, 220–224, and 327 exhibit low backbone fluctuations when compared to other more flexible domains (loops, terminal regions). It indicates that binding sites are structurally stabilized due to ligand binding. The residues Arg220, Phe224, Tyr327, Lys180, and Arg181 have low RMSF in these regions upon ligand interaction (Fig. S28C). It also overlaps with the interacting residues from the 3D ligand interaction diagram, indicating residues with low RMSF in the MD data. These results support the notion that QPyN16Ge binding stabilizes the functional site of the enzyme FemA. The findings indicate that QPyN16Ge binding to FemA may inhibit the pentaglycine cross-bridge, which is required for a stable peptidoglycan cell wall in *S. aureus*. The dramatically reduced crosslinking could result in a highly disordered, structurally degraded peptidoglycan meshwork that cannot withstand the high internal osmotic pressure of the bacterial cell. This results in the release of cellular content, ultimately leading to cell death, as supported by investigations of membrane integrity and scanning electron microscopy (Fig. 2 and Fig. 3).

Table S2: Glide XP docking scores of screened compounds.

	Docking score (kcal/mol)			
Compound	1LRZ	1MWT	3VMT	6FTB
QPyN16Ge	-5.449	-0.141	-2.504	0.215
QPyN18Ge	-5.178	-2.179	-1.129	1.063
QPyN14Ge	-4.575	1.126	-2.729	-1.599
QPyN12Ge	-4.246	-4.382	-2.444	-1.48
QPyN10Ge	-3.842	-3.517	-1.966	-1.746